*applied sciences*

MDPI

*Article*

# Durability Enhancement of Coal-Fired Biomass Ash Concrete Using Bio-Inspired Self-Healing Coatings

**Nisal Dananjana Rajapaksha [1], Mehrdad Ameri Vamkani [1], Zarina Yahya [2], Rahul V. Ralegaonkar [3], Michaela Gkantou [1], Francesca Giuntini [4] and Ana Bras [1,*]**

[1] Built Environment and Sustainable Technologies (BEST) Research Institute, Liverpool John Moores University, Byrom Street, Liverpool L3 3AF, UK; r.y.dananjana@2023.ljmu.ac.uk (N.D.R.); m.amerivamkani@ljmu.ac.uk (M.A.V.)
[2] Faculty of Civil Engineering & Technology, Universiti Malaysia Perlis (UniMAP), Perlis 01000, Malaysia
[3] Department of Civil Engineering, Visvesvaraya National Institute of Technology, Nagpur 440010, India
[4] Pharmacy and Biomolecular Science, Liverpool John Moores University, Liverpool L3 3AF, UK
* Correspondence: a.m.armadabras@ljmu.ac.uk

**Abstract**

Premature deterioration of reinforced concrete is driven largely by moisture and chloride ingress, which accelerate steel corrosion and shorten service life. This study investigates a dual strategy to enhance durability while supporting circular-economy goals: (i) incorporating coal-fired biomass ash (CBA) as a fine-aggregate replacement (0%, 20%, and 50%) and (ii) applying bio-inspired surface treatments to reduce transport pathways. To capture variability in CBA performance across different environmental and material contexts, two concrete systems—produced in India and the UK—were evaluated, each subjected to a distinct coating approach: a bacterial self-healing treatment or a cinnamaldehyde (CNM) organic barrier. Mechanical, transport, and multi-scale characterization was performed, including compressive strength, capillary absorption, chloride migration (NT Build 492), SEM/EDS, XRF, and XRD. The 20% CBA mixes maintained or slightly improved strength, while higher CBA contents increased porosity but reduced chloride transport in the UK mix. The bacterial coating reduced long-term water absorption by over 80% through $CaCO_3$ mineralization, offering strong moisture resistance. The CNM coating decreased chloride migration by up to 68% via hydrophobic and ionic-blocking effects. Overall, moderate CBA with self-healing treatment enhances moisture control, whereas higher CBA with CNM provides effective chloride protection, extending the service life of CBA-based concrete.

**Keywords:** self-healing concrete; cinnamaldehyde; coal fired-biomass ash; chloride migration; capillary absorption; SEM/EDS–XRD



Academic Editor: Markssuel Teixeira Marvila

Received: 21 January 2026
Revised: 20 February 2026
Accepted: 23 February 2026
Published: 28 February 2026



## 1. Introduction

### 1.1. Background and Motivation

Concrete underpins global infrastructure, but its durability is frequently compromised by reinforcement corrosion, moisture ingress, and cracking, with corrosion costs estimated at around 3–4% of global GDP [1] and substantial avoidable expenditure when corrosion management is improved. Reinforced concrete's high-alkalinity pore solution passivates steel; however, carbonation and chloride ingress can de-passivate or locally break the passive film, accelerating damage, loss of serviceability, and costly repairs [2,3]. At the same time, the cement industry remains a major source of $CO_2$. Process and energy emissions

from cement manufacture contribute a notable share of global anthropogenic $CO_2$ (historically ~4% for process emissions alone, with total sector emissions commonly reported in the 6–8% range depending on year and accounting method) [4,5]. Reducing clinker content and valorizing industrial by-products are therefore critical pathways towards durable, sustainable construction. Transforming local, landfill-destined waste, including co-fired biomass ash (CBA), into construction materials is vital for reducing GHG emissions [5,6].

The construction sector is exploring coal-fired biomass ash (CBA)—a by-product of co-firing biomass and coal—as a viable supplementary cementitious material that aligns with circular-economy targets. CBA offers the potential to reduce natural aggregate extraction and cement demand, yet its composition and reactivity vary significantly depending on fuel mix, combustion technology, and geographic sourcing emissions [5,6]. This variability raises essential questions about its influence on concrete durability, particularly when exposed to harsh environments. A central challenge in extending RC service life is controlling the ingress of water and chlorides, which are the major triggers for corrosion initiation. Conventional surface treatments—polymeric coatings, silanes/siloxanes, epoxy layers, and chemical corrosion inhibitors—offer temporary protection but are prone to degradation under UV radiation, abrasion, and chemical exposure. More advanced measures, such as cathodic protection or stainless-steel reinforcement, are effective but economically prohibitive for widespread use. Recent research has shifted toward bio-inspired and environmentally benign coatings, including bacteria-based self-healing systems, which induce $CaCO_3$ precipitation to seal cracks and block transport pathways [2,7], and natural organic inhibitors such as cinnamaldehyde, which form hydrophobic or chemisorbed layers capable of delaying chloride penetration. These nature-derived strategies offer a promising pathway toward passive, autonomous, and low-carbon corrosion mitigation. This study investigates two complementary approaches to mitigating premature deterioration of concrete incorporating CBA:

1. Enhancing material sustainability through partial replacement of fine aggregates with CBA (0%, 20%, and 50%).
2. Improving durability performance using two bio-inspired surface treatments:
    a. A bacteria-based self-healing coating;
    b. A cinnamaldehyde (CNM) organic corrosion-inhibiting barrier.

To capture real-world variability in CBA behavior across different climatic and sourcing conditions, the research intentionally evaluated two distinct concrete systems—one prepared in the UK and another in India—each subjected to one of the coatings. This design enables us to examine how CBA interacts with both environmental context and surface treatment, rather than directly comparing the two coatings under identical conditions. The rationale is not to rank coatings against each other, but to understand how different bio-inspired strategies can be paired with CBA concrete depending on local performance priorities—moisture control or chloride resistance.

### *1.2. Sustainable Concrete with CBA*

CBA has emerged as a potential supplementary cementitious material (SCM), produced from the co-combustion of coal and biomass. In Europe, the increasing practice of co-firing coal with diverse biomass, such as wood chips and sawdust, has led to a burgeoning generation of CBA [8] to reduce the reliance on fossil fuel for electricity generation, an approach to reduce GHG emissions and cost/consumption of raw materials, fostering a circular economy. CBA derived from locally available agro-industrial by-product [9] from the co-firing of coal, rice husk, wood chips, and sawdust, constitutes a critical waste stream with immense potential for valorisation in sustainable construction materials [10]. Depending on chemical characteristics, mineral phases, and particle size, CBAs can be

used as a precursor, binder, or sand replacement. CBA has emerged as a potential supplemental cementitious material (SCM), produced from the co-combustion of coal and biomass. Replacing 25% of the cement with CBA gives the concrete compressive and flexural strengths that are similar to those found in conventional fly ash concretes [11]. Conversely, lower concentrations increase the concrete's resistance to chloride and decrease its propensity to absorb water [12]. However, biomass ash is not always the same and has significant amounts of alkali content (which can cause alkali–silica reactions), and using CBA can reduce cement consumption and carbon footprint while maintaining or improving durability [6,11]. Properly engineered, co-fired ashes can perform comparably to coal fly ash in fresh and hardened properties and improve durability metrics, including chloride resistance. Yet, concrete made with ash replacements may exhibit higher porosity, permeability, or alkali variability depending on source and dose, challenging durability in aggressive environments [10]. Coatings and surface treatments are therefore attractive adjuncts to control ingress. Traditional repair/coating strategies can suffer from limited life under UV, abrasion, and chemical attack, or interface incompatibilities, motivating autonomous/self-healing approaches as complementary solutions [13].

To address the significant economic and structural challenges posed by concrete degradation, bacteria-based self-healing coatings have emerged as a promising, sustainable solution for autonomous corrosion control, crack repair, and a novel opportunity for waste utilization [2,7]. RC corrosion costs £23 billion a year in the UK alone [3]. Therefore, the corrosion resistance of steel reinforcement is an important component of the lifecycle of RC. The pore solution of fresh concrete has a pH of 12.5 to 13.5, which makes steel inert and develops a stable oxide layer against chlorides [14]. But carbonation or chloride infiltration can damage its protection. Carbonation reduces pH as atmospheric $CO_2$ reacts with calcium hydroxide, destabilizing the passive layer below pH 9.5 [15]. Chlorides, prevalent in marine and de-icing agents, disrupt the protective film at certain locations and initiate pitting corrosion, even under alkaline conditions, which rapidly results in cracking and spalling [14]. As a result, structures that are supposed to endure 50 to 100 years frequently fall apart in just a few decades, which means they need costly repairs and replacements [16].

Self-healing concrete (SHC) is a proactive approach based on biological systems that allows cracks to seal themselves and make the material stronger. Microencapsulation and bacterial self-healing are the two basic ways. Microencapsulation uses capsules with healing agents inside them. When the capsules break, they release compounds that fix cracks and make the material less permeable [17]. The main drawbacks of microencapsulation are fragility and the single use [18]. Microbiologically induced calcium carbonate precipitation (MICP) is the mechanism underlying bacteria-based self-healing concrete (SHC). It uses spores of Bacillus subtilis or Sporosarcina pasteurii that precipitate $CaCO_3$ when reached by water, sealing cracks and making the microstructure denser [19,20]. Studies indicate permeability reductions reaching 55% and delayed chloride ingress [3,21], which reduces maintenance requirements, resulting in decreased lifecycle carbon emissions [3]. SHC technologies are still in the early stages of development, even though they provide many benefits. High production costs, bacterial viability challenges, and uncertainties in large-scale applications limit the acceptability [22]. Parallel to SHC, bio-inspired coatings (e.g., plant-derived polymers, essential-oil constituents) have been explored to provide hydrophobic barriers and corrosion inhibition with lower toxicity than nitrite-based systems [23]. Most traditional corrosion inhibitors, such as nitrites, increase the cost and risk of toxicity [14]. Plant extracts that include neem (Azadirachta indica) and turmeric (Curcuma longa) were shown to inhibit corrosion through the formation of films that adhere to steel [24,25]. Within this space, cinnamaldehyde—the principal component of cinnamon oil—has demonstrated corrosion inhibition via adsorption and film formation on steel and

has been evaluated in cementitious systems using lightweight aggregates (LWAs) as carriers to avoid hydration retardation when used directly as an admixture. Evidence shows longer time to cracking in accelerated tests and improved chloride thresholds/sorptivity with cinnamaldehyde–LWA delivery, although trade-offs in early-age strength and setting have been observed. Cinnamaldehyde is the primary active ingredient in cinnamon oil that extracted from cinnamon bark, and cinnamaldehyde is identified as a natural corrosion inhibitor [26,27]. It has been shown that cinnamaldehyde delays the cement hydration when it is used as a direct admixture [27], but [28] proposed soaking lightweight aggregates in cinnamaldehyde. This delayed-release technique maintains the early hydration and enhances chloride thresholds, lowering sorptivity by enabling the chemical to build protective layers on rebar [28]. However, these cinnamon-based solutions remain investigational, but they demonstrate innovative, bio-inspired approaches.

The cinnamon industry around the world produces around 577 million tonnes of waste each year [29], and only 10% of that is recycled. Transforming about 200 kilotons of cinnamon by-products into corrosion inhibitors is a green, renewable option to synthetic agents that also helps the goals of a circular economy [29]. Further research is required to enhance healing efficacy, ensure compatibility with SCMs such as CBA, and evaluate its long-term durability in real-world conditions. Although both cinnamaldehyde and bacteria-based self-healing technologies demonstrate promise for corrosion mitigation, their combined implementation within bio-concrete remains largely unexplored.

Traditionally, organic admixtures like blood, oils, and fats were added to mortars to increase workability and water resistance [30,31]. Modern research has expanded on this by evaluating the effect of plant extracts, essential oils, and biopolymers. These materials are appealing due to their availability, renewability, and non-toxicity [30,32]. Other natural biopolymers, which are polysaccharides like guar gum, cactus mucilage, and okra extract, have the potential to improve water retention, reduce shrinkage, and increase strength [30,33]. The polysaccharide and protein content of cactus extract modified concrete resulted in increased strength and decreased permeability [33]. Low percentages of chitosan from seafood waste (0.05%) enhanced compressive strength and densified the microstructure [34]. Also, the reviews show that natural polymers can increase mechanical characteristics and durability by up to 30% at low doses [30,32]. The bio-inspired coatings, such as superhydrophobic layers, resist water by mimicking lotus leaves using eco-friendly waxes and biomimetic polymers [31]. These can significantly minimize the ingress of chlorides and penetration of water while increasing durability. However, variability in natural substances, supply scalability, and long-term field data remain challenges [32].

While SHC and cinnamaldehyde-based approaches have been studied independently, there is limited evidence on their direct comparison as surface treatments on CBA-modified concretes, and on how coating mechanism (mineralizing vs. hydrophobic/inhibitive) interacts with CBA dosage to affect water absorption and chloride migration (NT Build 492), alongside microstructural/mineralogical changes. The research gap addressed in this work lies at the intersection of (i) sustainable concrete with CBA, (ii) bio-inspired protective surface treatments, and (iii) multi-environment durability assessment. This study investigates the incorporation of cinnamaldehyde and self-healing bacteria into concrete formulations, focusing on optimizing distribution methods, minimizing impacts on mechanical properties, and assessing long-term durability under environmental conditions. The investigations strive to promote a sustainable, corrosion-resistant concrete system that optimizes the use of locally available resources, such as CBA.

## 2. Materials and Methods

### 2.1. Materials for Concrete

#### 2.1.1. Cement

This study used Ordinary Portland Cement (OPC) type one cement (CEM I) as per BS EN 197-1 standard [35]. The strength class is 52.5 N. CEM I cement, which is widely used in a variety of applications in the industry [2].

#### 2.1.2. Aggregates

The fine aggregate was selected to comply with the ASTM C33/EN 12620 [36,37]. The material was oven-dried, sieved remove particles larger than 4.75 mm, and tested for grading, specific gravity, and fineness modulus to guarantee compliance with concrete mix specifications.

The coarse aggregate used in this research had nominal particle sizes of 10 mm and 20 mm. The aggregate was washed, surface-dried, and tested for water absorption, specific gravity, and grading in accordance with ASTM C33/EN 12620 to ensure its suitability for structural concrete.

#### 2.1.3. Coal-Fired Biomass Ash (CBA)

Coal-fired biomass ash (CBA) (as shown in Figure 1) is a locally available industrial by-product in the city of Nagpur, India, used as a fine aggregate replacement in concrete mixtures. CBA was collected in a dry state from a coal-fired power station in Nagpur. Chemical composition and grain size distribution of CBA are presented in Table 1 and Figure 2.

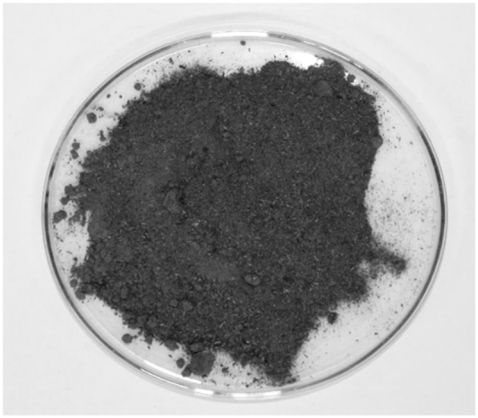

**Figure 1.** Co-fired biomass ash (CBA).

**Table 1.** Chemical composition of the CEM I and CBA used in the concrete production.

| Chemical Analysis | CEM I | CBA |
|---|---|---|
| $SiO_2$ | 21.02 | 23.6 |
| CaO | 64.73 | 51.22 |
| $Al_2O_3$ | 5.15 | 1.68 |
| $Fe_2O_3$ | 3.43 | 1.11 |
| MgO | 0.55 | 1.91 |
| $K_2O$ | 0.64 | 1.87 |
| $Na_2O$ | 0.27 | 2.1 |
| $TiO_2$ | 1.33 | 1.23 |
| $P_2O_5$ | 0.87 | 0.25 |
| MnO | 0.15 | 0.075 |
| Cl | | 0.04 |

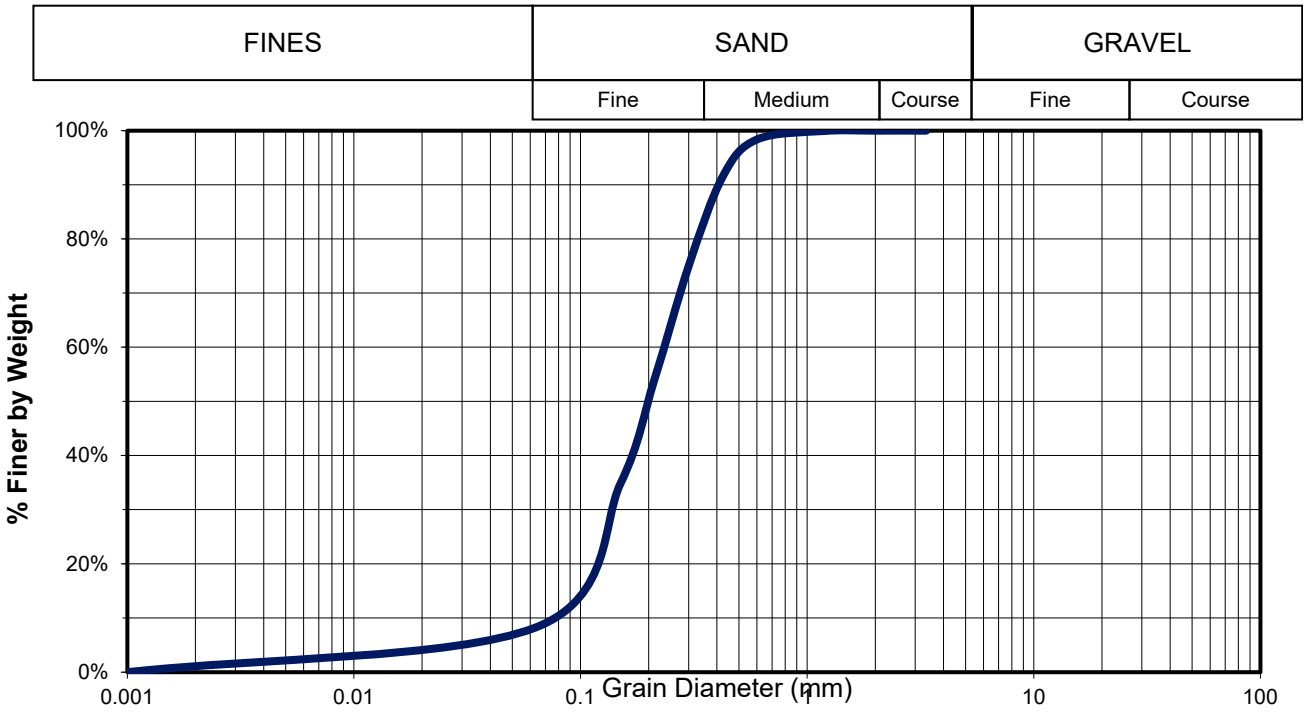


**Figure 2.** Grain size distribution of the CBA used in concrete.

### 2.2. Materials for CBA Concrete and Bio-Coating Application

CBA was used as a partial replacement for fine aggregates in 20% and 50% in concrete production. Two different concretes were produced: one in India (0, 20%, and 50%) and another one in the UK (also using the 0, 20%, and 50% of CBA replacement) (Table 2). A total of 3 cubes and 6 cylinders of each composition were then cast.

**Table 2.** Mix proportions of the concrete.

| | Produced in India | | | Produced in the UK | | |
|---|---|---|---|---|---|---|
| **CBA** | **0%** | **20%** | **50%** | **0%** | **20%** | **50%** |
| **Concrete Composition** | **kg/m$^3$** | **kg/m$^3$** | **kg/m$^3$** | **kg/m$^3$** | **kg/m$^3$** | **kg/m$^3$** |
| CEM I | 387 | 387 | 387 | 450 | 450 | 450 |
| Agg. 20 mm | 1158 | 1158 | 1158 | 712 | 712 | 712 |
| Agg. 10 mm | 0 | 0 | 0 | 610 | 610 | 610 |
| Sand | 670 | 536 | 335 | 335 | 268 | 167.5 |
| CBA | 0 | 134 | 335 | 0 | 67 | 168 |
| water | 184 | 184 | 184 | 232.65 | 232.65 | 278.1 |
| w/c | 0.48 | 0.48 | 0.48 | 0.45 | 0.45 | 0.45 |

Two families of concretes were produced using the same India CBA: (i) an India housing-grade mix (≈M25) focusing on sand replacement, and (ii) a UK infrastructure-grade mix (≈C30/37) aligned with BS 8500 [38] exposure classes. This was designed to reveal substrate-specific interactions between CBA content and surface treatments under distinct performance baselines.

All concrete specimens were water-cured for 28 days after casting in 2019 and subsequently stored under laboratory conditions; surface coatings were applied approximately six years after casting on fully matured concrete.

2.2.1. Self-Healing Concrete Bio-Coating Components

This research utilized a strain of *Shewanella oneidensis* with Tryptic Soy Broth (TSB) used as a nutrient-rich medium to facilitate bacterial growth. TSB contains pancreatic digest of casein (17 g/L), papaic digest of soybean meal (3.0 g/L), sodium chloride (5.0 g/L), di-basic potassium phosphate (2.5 g/L), and glucose (2.5 g/L). The *Shewanella* strain was transferred to TSB that had been sterilized using autoclaving at 121 °C for 20 min and subsequently cooled. Following that, the bacteria culture was placed in a shaking incubator for a duration of 19 h at a temperature of 30 °C and a speed of 200 rpm in order to produce a liquid bacteria solution (bioproduct). Following incubation, the number of colonies was counted using the serial dilution technique, resulting in a colony-forming unit per milliliter (CFU/mL) of 108 CFU/mL in the bacteria solution.

The initial dry weight of each concrete cookie sample (dia. 100 mm, thk. 50 mm) was measured. The concrete samples were then sterilized using an autoclave. After sterilization, the weight of each sample was measured again. All samples, along with a weighing scale and storage boxes, were placed inside a fume cabinet. The bacterial solution was poured into the box, and a 2 mm thickness of the solution was maintained, as shown in Figure 3. The solution was left with the samples for 10 min. After this period, the samples were weighed again. The control samples were placed in a separate box. Each control sample received 2 mm of sterile distilled water, following the same process as the treated samples. These control samples were also weighed after 10 min.

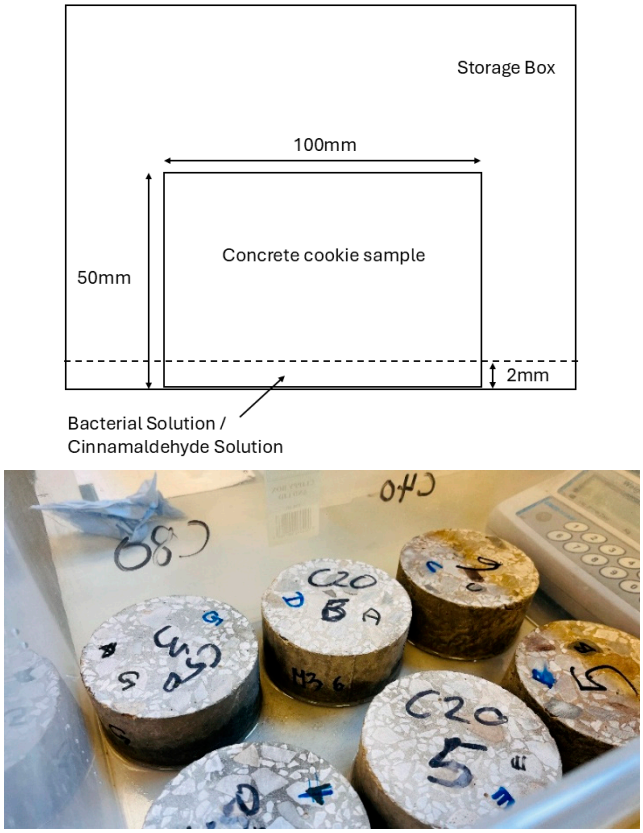


**Figure 3.** Bacterial solution/cinnamaldehyde coating process applied to fully matured concrete specimens (28-day cured; approximately six years old at the time of coating).

All samples were placed upside down in the boxes, with the treated surface facing upwards. Distilled water was added to each box to a level equal to one-third of the sample height. The boxes were then sealed and placed in an incubator at 30 °C for 10 days. After

incubation, the samples were removed from the boxes. Drying was carried out with the treated surface facing upwards until a constant weight was achieved.

#### 2.2.2. Cinnamaldehyde Coating Components (CNM)

Cinnamaldehyde (C9H8O) is the major component of cinnamon oil, comprising approximately 80% to 94.8% of its chemical composition. Cinnamon (Cinnamomum verum) is a popular food and pharmacological ingredient that can be extracted from bark, leaves, or waste (Figure 4).

**Figure 4.** Cinnamon wood waste (**left**) and leaves (**right**).

Cinnamon contains several bioactive qualities, such as antibacterial, anti-inflammatory, antioxidant, and cardioprotective actions [39]. Cinnamaldehyde solution was ordered from sigma Aldrich [40]. Table 3 and Figure 5 show the technical data of the cinnamaldehyde solution [40].

**Table 3.** Technical data of cinnamaldehyde sample [40].

| Cinnamaldehyde | 3-Phenylprop-2-Enal |
|---|---|
| Formula | C6H5CH=CHCHO |
| Molecular Weight | 132.16 |
| CAS-No. | 104-55-2 |
| EC-No. | 203-213-9 |
| Physical state | Liquid |
| pH | 4.7 at 30 °C |
| Water solubility | 2.865 g/L at 25 °C |
| Density | 1.05 g/cm$^3$ at 20 °C |
| Biological Source | Cassia oil |

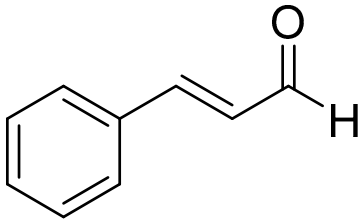


**Figure 5.** Cinnamaldehyde [40].

The initial dry weight of each concrete disk sample was measured. The samples were sterilized using an autoclave. After sterilization, the weight of each sample was measured again. All samples, along with a weighing scale and storage boxes, were placed inside a fume cabinet. Each concrete sample was placed inside a separate box. The cinnamaldehyde solution was poured into the box and maintained 2 mm thickness of the solution, as shown

in Figure 3. The solution was left with the samples for 15 min. After this period, the samples were weighed again. All samples were placed upside down in the boxes with the cinnamaldehyde-coated surface facing upwards. The boxes were sealed and placed in an incubator at 30 °C for 3 days. The samples were then removed and dried with the coated surface facing upwards until a constant mass was achieved.

### 2.3. Experimental Program and Testing Methods

Concrete mixes with 0%, 20%, and 50% CBA produced in India and in the UK were evaluated for compressive strength, water absorption, chloride migration [41], and microstructural changes using SEM/EDS, XRF, and XRD. Comparison was then made when using bio-inspired surface treatments: a bacterial self-healing coating and a cinnamaldehyde-based (CNM) organic barrier.

#### 2.3.1. Compressive Strength

The initial compressive strength was evaluated according to BS EN 12390-3:2009 [42] using 150 mm concrete cubes. The compressive strength test was done for 3 cubes of the same composition and age. The samples were subjected to compression testing in compliance with EN 12390-3 [42], and the compressive strength was determined based on the peak load at failure [2].

#### 2.3.2. Capillary Water Absorption

A capillary test was performed according to EN 1015-18:2002 [43] to assess short-term water absorption [2]. Concrete cylinders (100 mm × 50 mm) were dried at 30 °C until their weight difference was less than 0.1%, then immersed in 5 mm of water over absorbent paper in an airtight container, as shown in Figure 3. The weight was recorded at intervals (0′, 5′, 15′, 30′, 1 h, 2 h, 3 h, 24 h, and 14 days) until absorption stabilized. The water absorption coefficient was used to assess durability. Samples included control (0% CBA) and bio-product- or cinnamaldehyde-coated mixes with 0%, 20%, and 50% CBA.

#### 2.3.3. Chloride Migration Coefficient

The chloride migration coefficient was determined following NT Build 492 [41], according to Equation (1). Cylindrical specimens (100 mm diameter, 50 ± 2 mm thickness) were cleaned, surface-dried, and placed in a vacuum chamber at 10–50 mbar for 3 h, followed by immersion in a saturated calcium hydroxide solution under vacuum for 1 h. After 18 ± 2 h, the specimens were tested in a catholyte solution of 10% NaCl and an anolyte solution of 0.3 M NaOH. The specimens were sealed with rubber sleeves and stainless-steel clamps, and a DC voltage was applied as per NT Build 492 guidelines (Figure 6). Current and temperature were recorded at the start and end of the test. After that, the specimens were cleaned, axially split, and sprayed with 0.1 M silver nitrate solution. Then, the chloride penetration depth was measured at 10 mm intervals, excluding the 10 mm edge zones, with seven measurements taken per specimen to calculate the average penetration depth.

$$D_{nssm} = \frac{0.0239(273+T)L}{(U-2)t}\left(x_d - 0.0238\sqrt{\frac{(273+T)L\,x_d}{U-2}}\right) \quad (1)$$

where

$D_{nssm}$ = non-steady-state migration coefficient ($\times 10^{-12}$ m$^2$/s);
U = absolute value of the applied voltage (V);
T = average value of initial and final anolyte temperature (°C);
L = specimen thickness (mm);
$X_d$ = average chloride penetration depth (mm);

t = test duration (h).

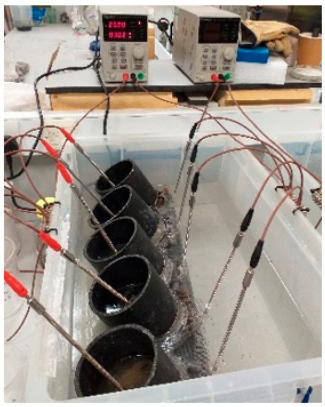

**Figure 6.** Chloride migration test according to NT Build 492 [41].

#### 2.3.4. SEM/EDS

Microstructural analysis was conducted using Scanning Electron Microscopy (SEM) and Energy Dispersive X-ray Spectroscopy (EDS) [2]. Concrete samples (~2 mm) were extracted from both coated and uncoated specimens, including both exposed surfaces and internal areas. A platinum coating was applied to each sample to improve electrical conductivity and imaging quality. SEM was used to assess crack structure and microstructural changes, while EDS provided elemental analysis to detect healing products and compositional variations due to the coatings.

#### 2.3.5. XRF

X-ray fluorescence (XRF) was used to analyze the chemical composition. The solid concrete samples with and without coatings were crushed into fine powders, dried, and formed into pellets. Both bulk concrete powders were made by grinding away the inside of concrete samples and the outside surface. The measurements were carried out using a Rigaku XRF spectrometer, and the analysis focused on determining the oxide composition of the samples to verify the chemical characteristics of CBA, concrete matrix, and coatings.

#### 2.3.6. XRD

X-ray diffraction (XRD) was used for mineralogical characterization. The samples from coated and uncoated specimens were powdered (less than 75 μm) and backloaded into holders. The powders extracted from the outside surface zones and the inside of the samples were examined by testing. The objective was to identify the crystalline phases of the CBA, hydrated cement products, and any self-healing or cinnamaldehyde-based compounds formed at the surface or within the bulk concrete because of the coating treatments.

## 3. Results and Discussion

### *3.1. Compressive Strength*

The results in Figure 7 summarize the average 28-day compressive strength of India and UK concrete samples with 0%, 20%, and 50% fine aggregate replacement by CBA.

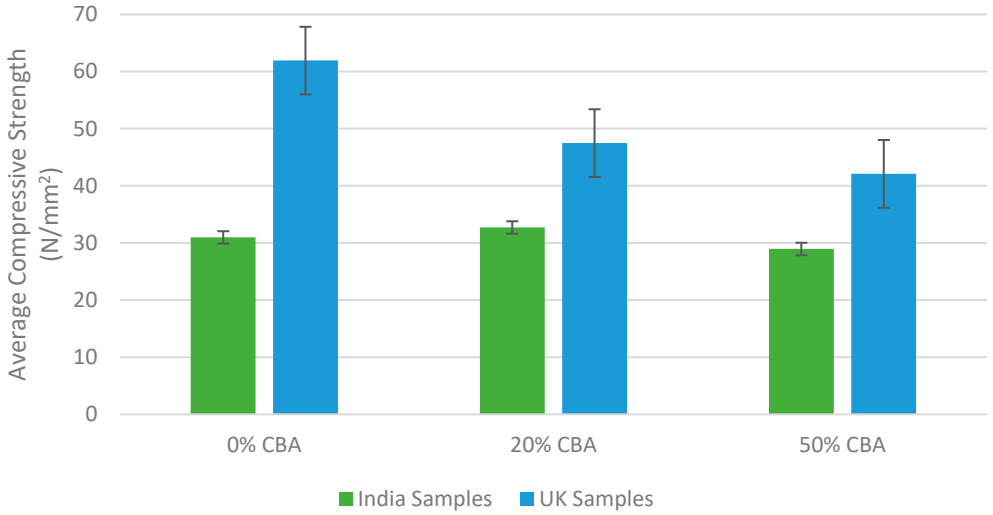


**Figure 7.** Average compressive strength of UK and India samples vs. CBA replacements at 28 days.

The India control samples (0% CBA) had an average strength of approximately 31 MPa. The concrete with 20% CBA increased the strength slightly to 32.7 MPa, which is 6% improvement in strength. However, 50% CBA replacement reduced the strength to 28.9 MPa, which is 6% lower than the control. But the UK control samples exhibited a higher strength of 61.9 MPa. The addition of CBA caused a significant reduction in strength at 20% CBA (47.5 MPa, a 23% decrease) and 50% CBA (42.1 MPa, a 32% decrease). Both mixes showed a downward trend at the 50% replacement level. But the UK concrete showed a significant reduction in strength with high CBA content compared to the Indian concrete.

These results suggest that the optimum CBA replacement level for maintaining compressive strength is approximately 20% or less. The small increase in strength at 20% CBA in the India mix aligns with previous studies showing that small amounts of CBA can act as micro-fillers or initiate secondary pozzolanic reactions by densifying the matrix [44,45]. The high control strength of the UK mix was significantly reduced with 20% CBA replacement, due to the porous nature of CBA particles disrupting the dense packing of the aggregate. At 50% replacement, both mixes experienced a clear strength drop, consistent with literature suggesting that replacing natural sand with bottom ash more than 30 to 50% weakens concrete [44]. The decrease in strength is attributed to the porous nature, because uneven CBA particles create a weak interfacial transition zone, which lowers aggregate packing density. CBA modifies the grading and particle packing of the fine fraction. At moderate replacement levels, finer ash particles may fill voids (filler effect), improving packing density. At higher replacement levels, increased porosity of ash particles and higher water demand may counteract this effect. Coal–biomass ashes may contain residual unburned carbon and volatile components, which can influence water demand, air entrainment, and strength development [46–48]. However, LOI/carbon content was not directly quantified in this study. The above justify the need to test bio-coatings aiming to improve CBA concrete durability.

### *3.2. Water Absorption*

Figures 8 and 9 show the water absorption via capillary of India and UK concrete with/without the two bio-coatings (self-healing and cinnamaldehyde) for 0, 20%, and 50% replacement of sand by CBA.

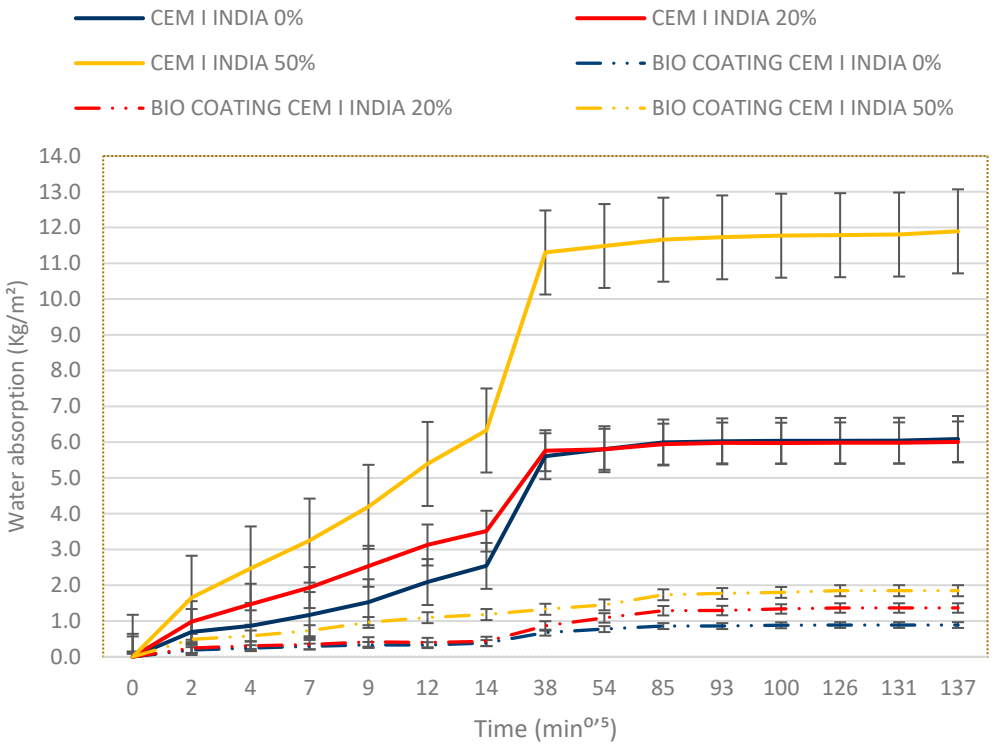


**Figure 8.** Capillary water absorption of Indian concrete with/without self-healing bio-coating.

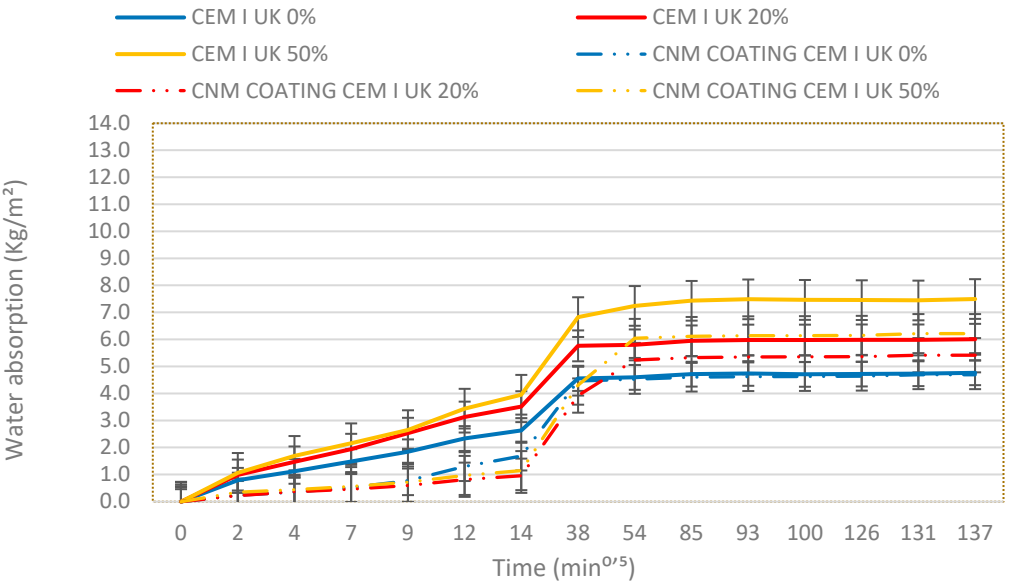


**Figure 9.** Capillary water absorption of UK concrete with/without cinnamaldehyde coating.

Country-specific effects were evident. In the India mixes, higher CBA raised capillary suction, but the self-healing coating consistently suppressed long-term uptake, indicating sustained mineralization within surface pores. In the UK mixes, the CNM coating effectively delayed early uptake yet offered limited long-term hydrophobicity, consistent with partial leaching of organic functionality over time.

The higher the quantity of the CBA is, the higher the water absorption detected for India and UK families. With increasing CBA content, non-coated Indian concretes seem to absorb more water with time, with a minimum of 6–12 kg/m$^2$ of absorbed water. However, the non-coated UK concrete compositions seem to present reduced water absorption for

the same concentration of CBA in comparison to the non-coated Indian concretes, with values ranging between 4.5 and 7.5 kg/m$^2$.

Bio-coatings clearly benefit CBA concretes. The self-healing coating improved all the Indian concretes tested by lowering the water absorption to values below 2 kg/m$^2$. Cinnamaldehyde coating also seems to decrease the speed of water absorption and maximum asymptotic value, but shows less inhibition of water absorption than the self-healing coating. According to Figure 8, in the first three hours, the water absorption increases rapidly until the pores are saturated, and then slows after the third hour. Higher CBA replacements caused an increase in water absorption in significant level. The India samples with 50% CBA show approximately 3.25 kg/m$^2$ in 30 min, exceeding the 0% CBA samples (1.168 kg/m$^2$ at 30 min). The UK samples also show the same pattern. These changes represent higher porosity and decreased hydration in high CBA-replaced concretes. According to literature, significant quantities of bottom or coal ash replacement enhance capillary absorption and decrease strength.

After three hours, the UK 0% CBA concrete absorbed much less water than the India 0% mix. This is because it had a higher compressive strength, a denser microstructure, and fewer connected pores because it had a lower water–cement ratio and better curing. In contrast, India samples continued absorbing water even after 24 h. Uncoated samples showed quick initial absorption and higher total intake, especially at 20% and 50% CBA. But the bio-product coating significantly reduced water uptake across all CBA levels. For Indian concrete, coated 0% CBA specimens absorbed only 0.29 kg/m$^2$ in 30 min compared to 1.17 kg/m$^2$ for uncoated samples (75% reduction), with 85% reduction after 13 days. Coated 20% and 50% CBA samples showed similar improvements. The 50% CBA specimens absorbed 1.85 kg/m$^2$, which is less than uncoated (11.9 kg/m$^2$). Through mineralization, such as calcium carbonate precipitation, the bio-product coating effectively sealed surface pores, obstructing capillaries and densifying the surface. This aligns with previous findings that bacterial self-healing agents reduce water absorption by forming mineralised barriers [2,49]. Overall, the coating kept Indian concretes nearly dry internally, demonstrating its effectiveness in enhancing durability and reducing moisture-related deterioration mechanisms, such as reinforcement corrosion, while the already dense UK concrete showed lower baseline absorption.

According to Figure 9, for the UK samples, the cinnamaldehyde coating significantly reduced early-stage water absorption but was less effective over the long term. At 30 min, the 0% CBA coated sample absorbed 0.52 kg/m$^2$ compared to 1.48 kg/m$^2$ for the uncoated sample, a 65% reduction, with 20% and 50% CBA mixes showing 70–80% reductions. This indicates that cinnamaldehyde initially acts as a hydrophobic barrier, filling surface pores and delaying water uptake. However, absorption of the 0% CBA coated sample increased to 4.46 kg/m$^2$ versus 4.55 kg/m$^2$ uncoated, and even at 50% CBA at 24 h, the reduction was only 17%. These results suggest the protective effect of cinnamaldehyde is temporary, likely due to leaching over time [27]. In comparison, the self-healing coating provided a stronger and longer-lasting defense. It reduced long-term water absorption by more than 80% across all mixes, indicating the formation of a continuous mineralised barrier that permanently blocked capillaries. While cinnamaldehyde offered only temporary pore sealing, the biomineral deposits effectively limited moisture penetration, enhancing durability and protection potentially against deterioration mechanisms such as reinforcement corrosion. This aligns with previous findings, highlighting that minimizing water absorption is critical for long-term concrete performance [49].

### 3.3. Chloride Migration

Figures 10 and 11 present the chloride migration coefficients of non-coated and coated UK and Indian concrete samples.

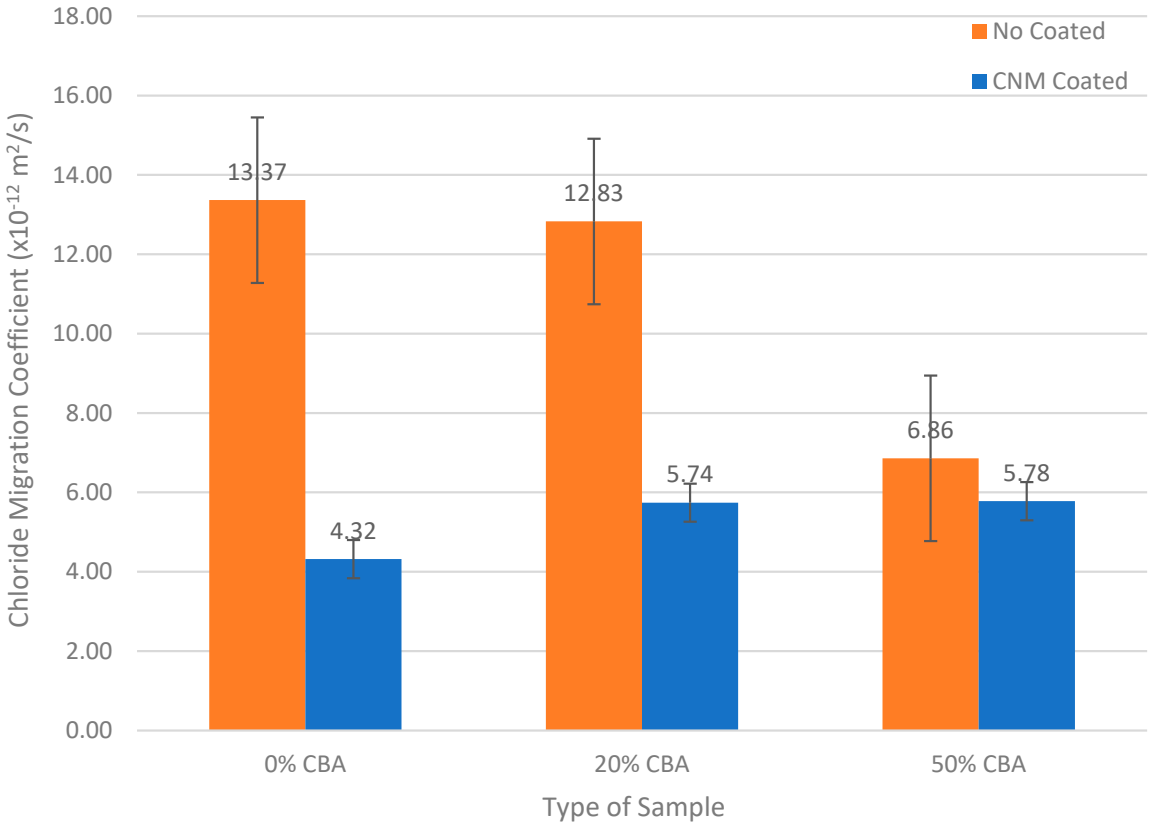


**Figure 10.** Chloride migration coefficients of cinnamaldehyde-coated and non-coated UK concrete samples.

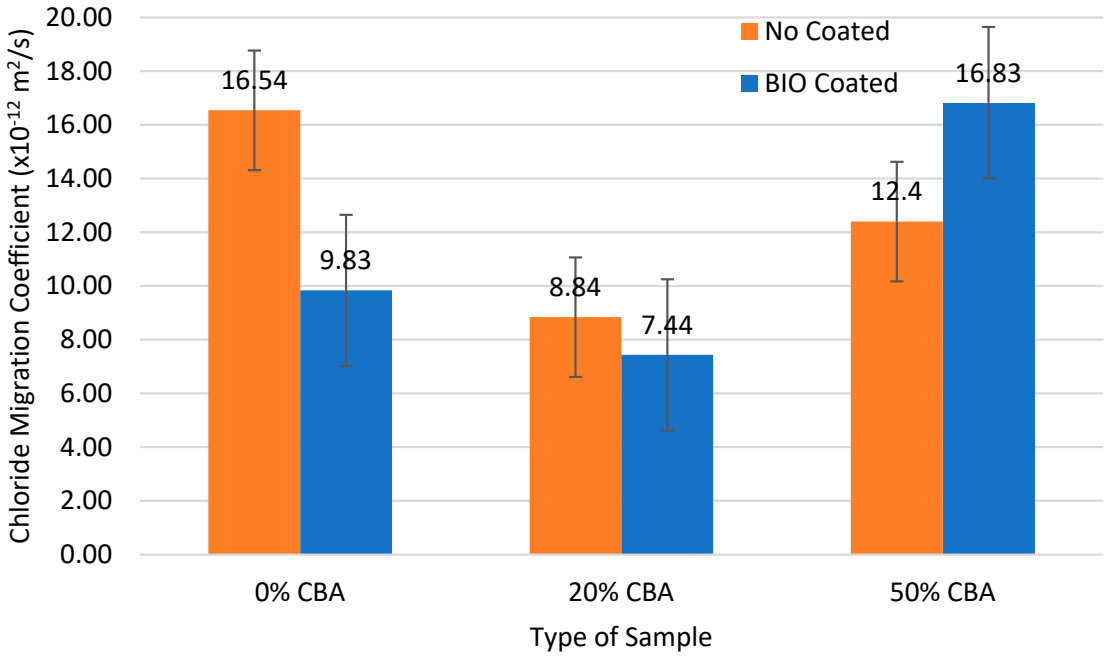


**Figure 11.** Chloride migration coefficients of self-healing coated (bio-coated) and non-coated Indian concrete samples.

For the UK concrete, the difference between adding 0% or 20% of CBA seems to be negligible, as the addition of 20% of ashes shows only a 4% reduction in the chloride migration. With a 50% CBA replacement, UK concrete exhibits the highest performance, achieving a 48.7% reduction in the chloride migration. This shows that the 50% CBA replacement is the most effective internal measure for chloride resistance, reducing the chloride migration coefficient into a range typically classified as "good resistance" (usually two to eight times 10–12 $m^2/s$). Although higher CBA contents increase total porosity, SEM analysis reveals that pore connectivity is significantly reduced, resulting in a more tortuous and discontinuous pore network that limits effective chloride transport.

For the Indian concrete, adding 20% of CBA leads to a decrease in the chloride migration of up to 46% in the Indian concrete, in comparison to the plain mix, suggesting that 20% CBA replacement (as a sand substitute) optimizes the particle packing and pore structure densification. The lower performance at 50% replacement may be attributed to higher capillary absorption, when a large proportion of ashes is used, where the 50% CBA replacement introduces detrimental microstructural effects, increasing the overall porosity and/or connectivity of the pore network. Figure 12 shows an example of the concrete samples exposed to chloride migration tests for 50% of CBA.

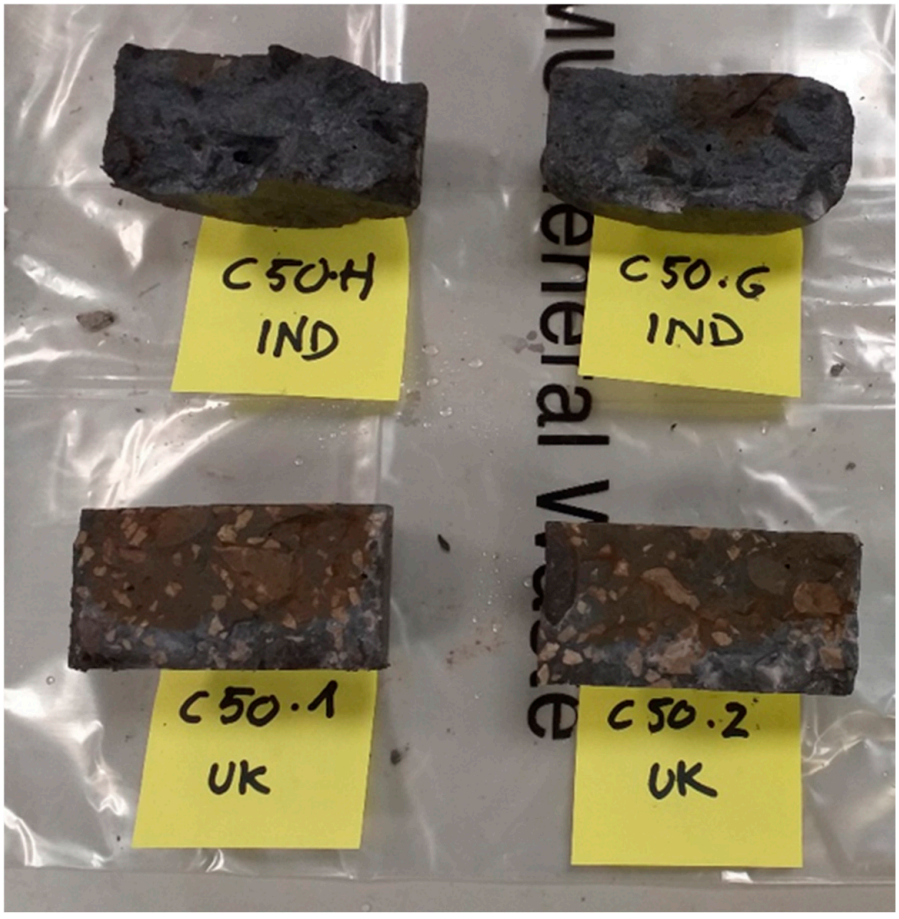


**Figure 12.** Some non-coated concrete samples exposed to chloride migration tests for 50% of CBA (India and UK samples).

The protective concrete bio-coatings with cinnamaldehyde and self-healing functionalities show different levels of chloride penetration. The UK concrete samples coated with cinnamaldehyde showed very low chloride ingress, and average penetration depths were about 10–20 mm, even at high CBA contents, as shown in Figure 9. This corresponds to incredibly low migration coefficients (D).

The cinnamaldehyde coating of the UK samples provides significant protection, primarily by reducing the migration coefficient by an average of 59.3% for the 0% and 20% CBA mixes. For all coated samples, the final $D_{nssm}$ values are close. This suggests that the coating dictates the final durability, and its benefit is largest for the least durable substrates.

The cinnamaldehyde (CNM) coating likely acts through a dual-mechanism approach, combining two primary methods of defense: physical pore blocking and chemical hydrophobicity.

The physical barrier and pore blocking mechanism is the most direct way for any coating to reduce the chloride migration coefficient. The CNM coating is a low-viscosity medium that allows it to penetrate the open pores, micro-cracks, and capillaries near the concrete surface. As the solvent evaporates or the CNM compound cures/polymerises, it forms a physical film within these pores. By filling the voids, this film significantly reduces the effective cross-sectional area through which chloride ions and water can travel. This forced detour or blockage is often the primary reason for the observed reduction in $D_{nssm}$ chloride ions, as they simply have fewer connected pathways to migrate under the applied electric field. The effectiveness of pore blocking is directly proportional to the density and depth of the film. A reduction from 13.37 (0% CBA) to 4.32 represents a 67.7% reduction and indicates a highly efficient barrier layer at the surface.

The chemical hydrophobicity is crucial for overall durability, as it addresses the water ingress problem. CNM is an organic compound (an aldehyde derived from cinnamon). When these organic coatings (or silanes/siloxanes) are used, they typically possess long, non-polar hydrocarbon chains. These chains can react or physically bond to the internal pore surfaces of the concrete (which are naturally hydrophilic). This chemical modification creates a hydrophobic (water-repellent) barrier in the pores. The surface energy of the pore walls is probably lowered to the point where the attraction between the concrete and water is less than the internal attraction of the water molecules themselves. Consequently, water is repelled, rather than being drawn into the concrete by capillary action. By repelling water and keeping the pores dry, the CNM coating drastically limits the amount of electrolyte (water) available, slowing the movement of chlorides even under the electric field created by the migration test [41].

Cinnamaldehyde and its derivatives are well-documented as corrosion inhibitors for steel [50]. They contain chemical groups (like the conjugated system and aldehyde group) that allow them to adsorb strongly onto the steel reinforcement surface. By forming a barrier that inhibits chloride penetration towards reinforcement, cinnamaldehyde was proven to delay the initiation of corrosion as an admixture or a surface treatment [51]. In this current study, cinnamaldehyde-coated samples indicated significantly higher resistant on chloride migration by indicating a low D value. This suggests that Cinnamaldehyde, as an eco-friendly and organic inhibitor, coated concrete surfaces may be a viable method of preventing corrosion.

The Indian concrete samples coated with self-healing functionalities had considerably higher D values in comparison to the CNN coating. However, for 0% CBA, the coated samples $D_{nssm}$ decrease substantially from 16.54 to 9.83 $\times 10^{-12}$ $m^2/s$. The coating successfully functions as a barrier, providing a 40.6% improvement in resistance. The replacement of sand by 20% of CBA in the Indian concrete mix still performs well, achieving the lowest overall $D_{nssm}$ of all the coated samples. However, the improvement compared to its uncoated counterpart is only 15.8%, indicating the coating's barrier effect adds less to an already durable substrate.

The deterioration of the 50% CBA sample's durability (16.83) is a major finding. The high content of porous CBA fines on the surface of the 50% CBA mix may negatively interact with the components of the bacteria culture medium, preventing proper curing,

self-healing, or adhesion, leading to a poorer overall barrier than the untreated concrete. The coating itself might be detrimental under these test conditions.

The bacteria-based self-healing coating significantly benefits the low-durability 0% CBA concrete. However, its performance is inconsistent and even detrimental at the 50% CBA content. The most effective product is the 20% CBA substrate combined with the bio-coating, achieving the lowest measured chloride migration coefficient.

Overall, chloride transport was governed by the interplay of substrate pore structure and coating mechanism. The 50% CBA UK mixes, despite strength loss, exhibited refined, less-connected pore networks favorable to CNM's ionic barrier, whereas the India 50% CBA mixes showed a heterogeneous microstructure that diminished the self-healing barrier efficacy.

### *3.4. Microstructural Analysis (SEM/EDS)*

SEM/EDS analysis was done in the center (IN) and on the border (OUT) of the concrete samples 0%, 20% and 50% of CBA produced in the UK (Figures 13 and 14) and in India before coating (Figures 15 and 16) and after coating with bacteria-based self-healing coating and CNM coating. Concrete is a heterogeneous composite material consisting of aggregates, cement paste, and interfacial transition zones (ITZs) [52]. Therefore, SEM observations presented herein distinguish between paste-dominated regions, aggregate particles, and ITZ areas. Dense regions observed in the micrographs may correspond to well-hydrated paste or aggregate phases.

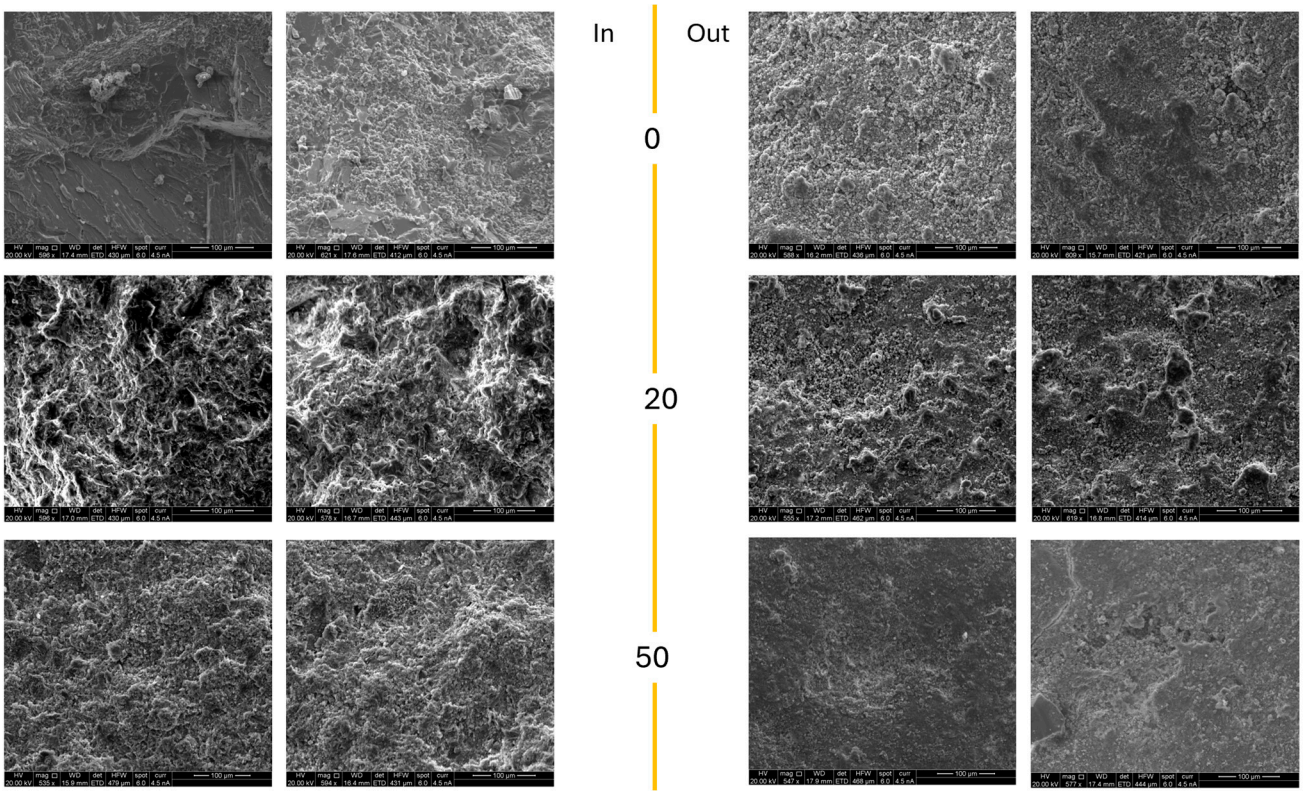


**Figure 13.** SEM analysis of the center (IN) and on the border (OUT) of the concrete samples 0%, 20% and 50% of CBA, produced in the UK, before coating.

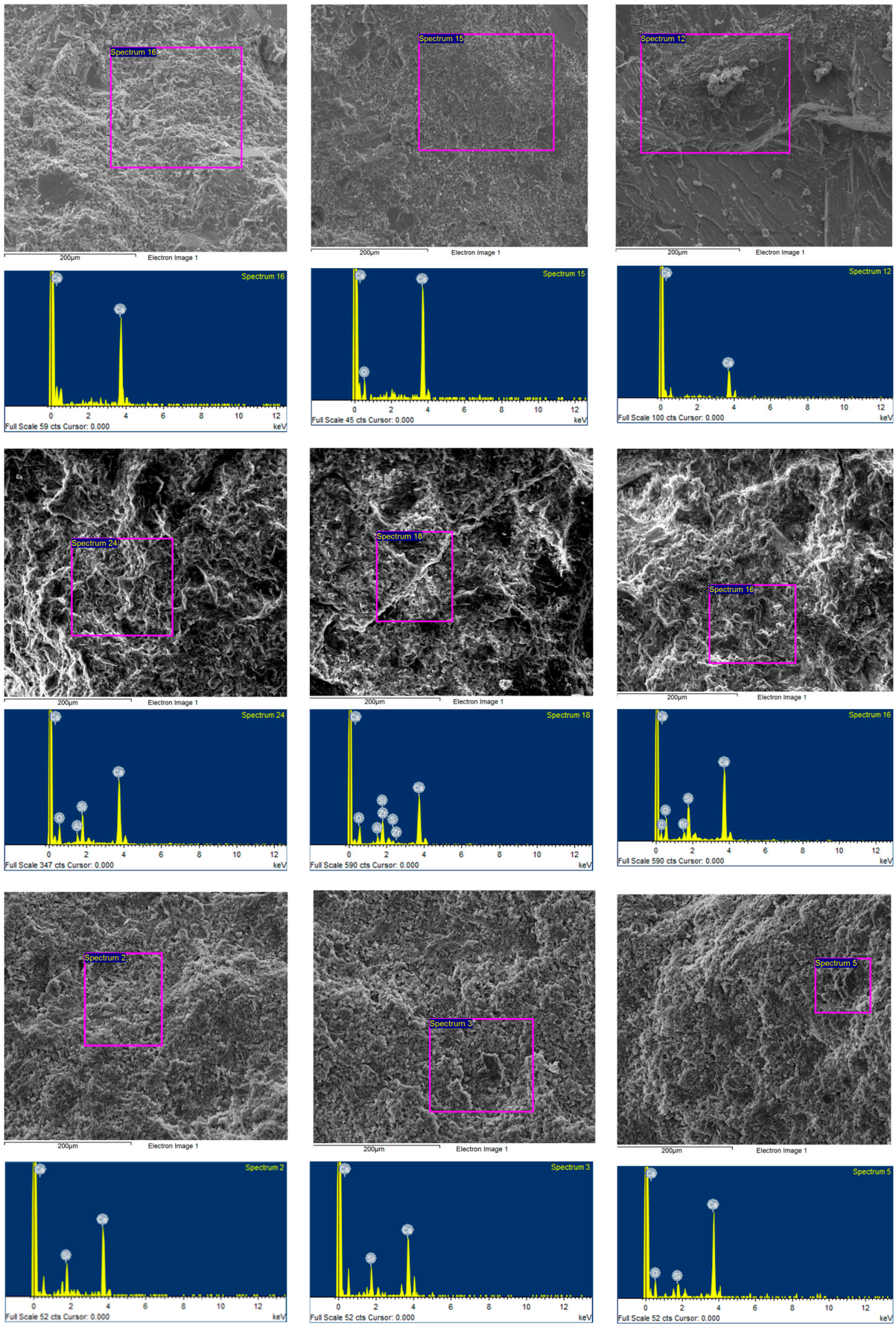


**Figure 14.** *Cont.*

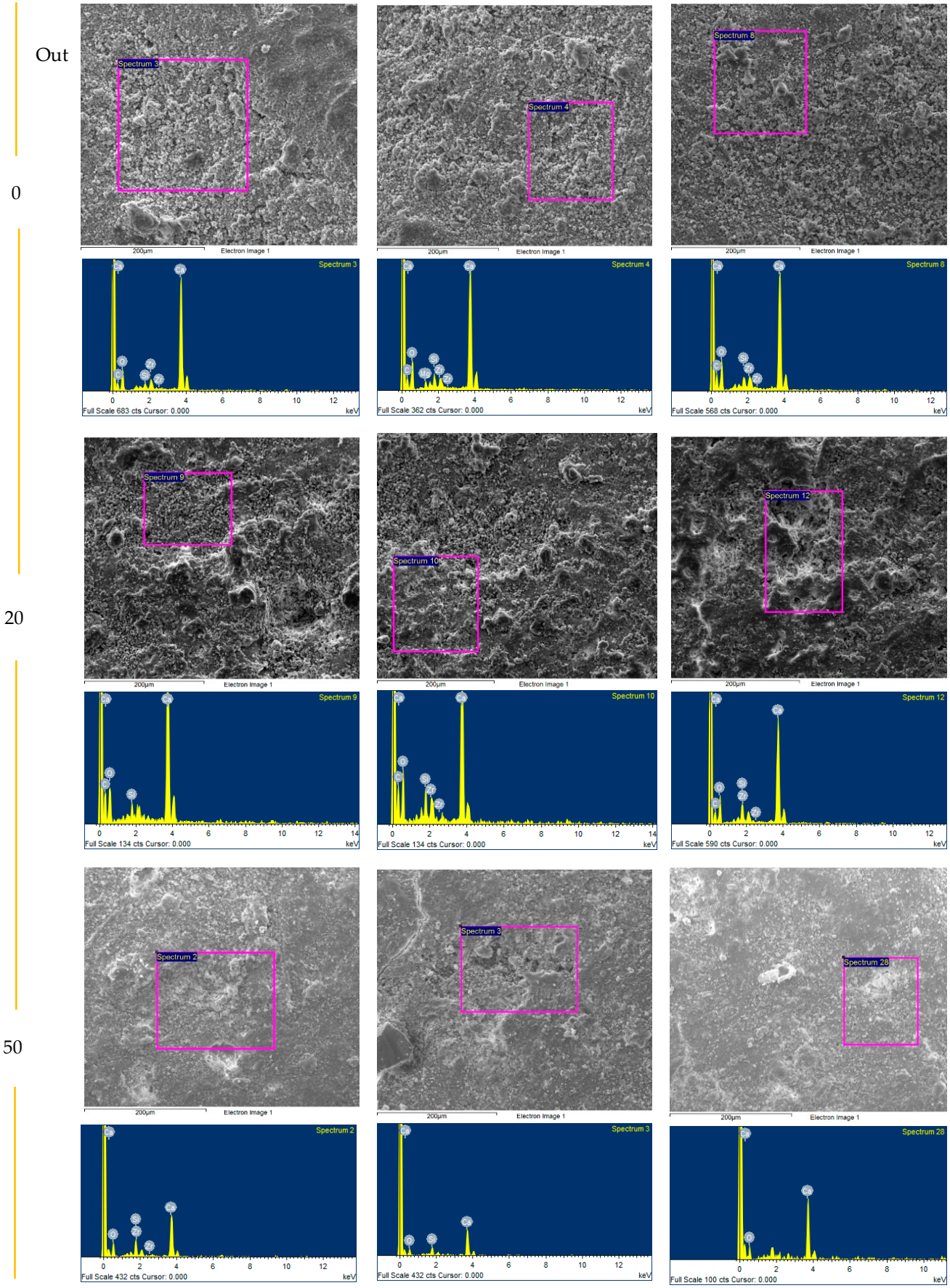


**Figure 14.** EDS (energy-dispersive X-ray spectroscopy) data for the UK's concrete, in the center (IN) and on the border (OUT) of the concrete samples 0%, 20%, and 50% of CBA before coating.

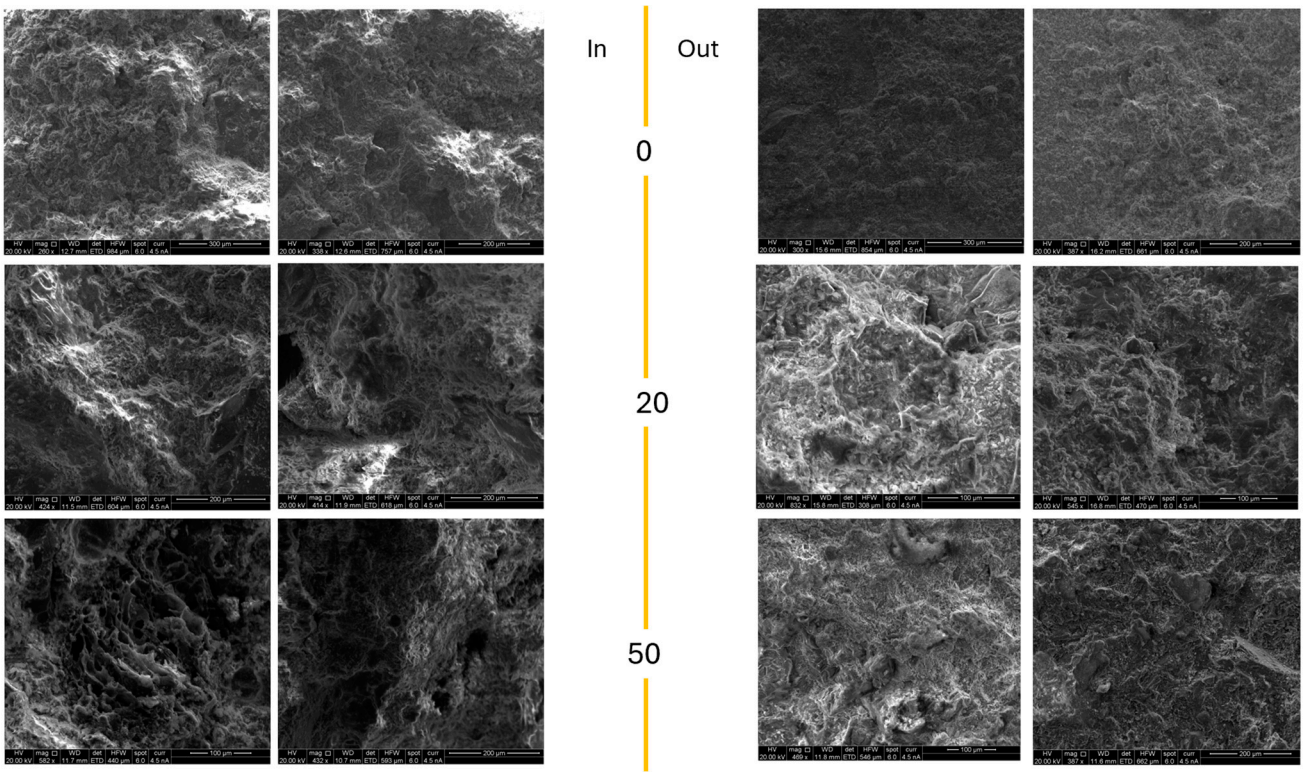


**Figure 15.** Analysis of the center (IN) and on the border (OUT) of the concrete samples 0%, 20% and 50% of CBA, produced in India, before coating.

#### 3.4.1. Before Coating

SEM analysis of the UK concrete before coating outer surfaces in 12 shows that the 0% CBA specimen has a porous microstructure with several interconnected cavities, which could provide paths for penetration. The 20% CBA specimen exhibits substantially fewer pores and a denser microstructure, indicating improved pore refinement compared to the control. At 50% CBA, the paste-dominated regions appear less porous, but significant microcracks are visible, suggesting that higher replacement levels induce internal stresses and weaker interfacial zones.

Considering the results of chloride migration (Figure 10), the UK concrete with 0% CBA shows a porous structure, with large features, well-connected capillary pores, and voids. The C-S-H gel structure is loose (Figure 14, 0% CBA). The porosity forms a percolation pathway (a continuous network) that allows chloride ions to traverse the material easily and rapidly.

However, for the UK concrete with 20% CBA, SEM results (Figure 14) show a slightly densified microstructure, with some localized filling of voids by CBA particles visible, but the large-scale connectivity of the capillary pore system remains intact. It seems that the "filler effect" at this low dose is insufficient to break the continuous network, with small benefits from the durability perspective.

The UK concrete 50% CBA (Figure 14) shows a highly densified microstructure, where large pores are nearly eliminated, replaced by disconnected nano-pores. The C-S-H matrix is smooth, uniform, and monolithic. As a result, the pore network is discontinuous (percolation is broken). Chloride ions are forced into a much longer, highly tortuous path, sharply reducing the effective migration rate.

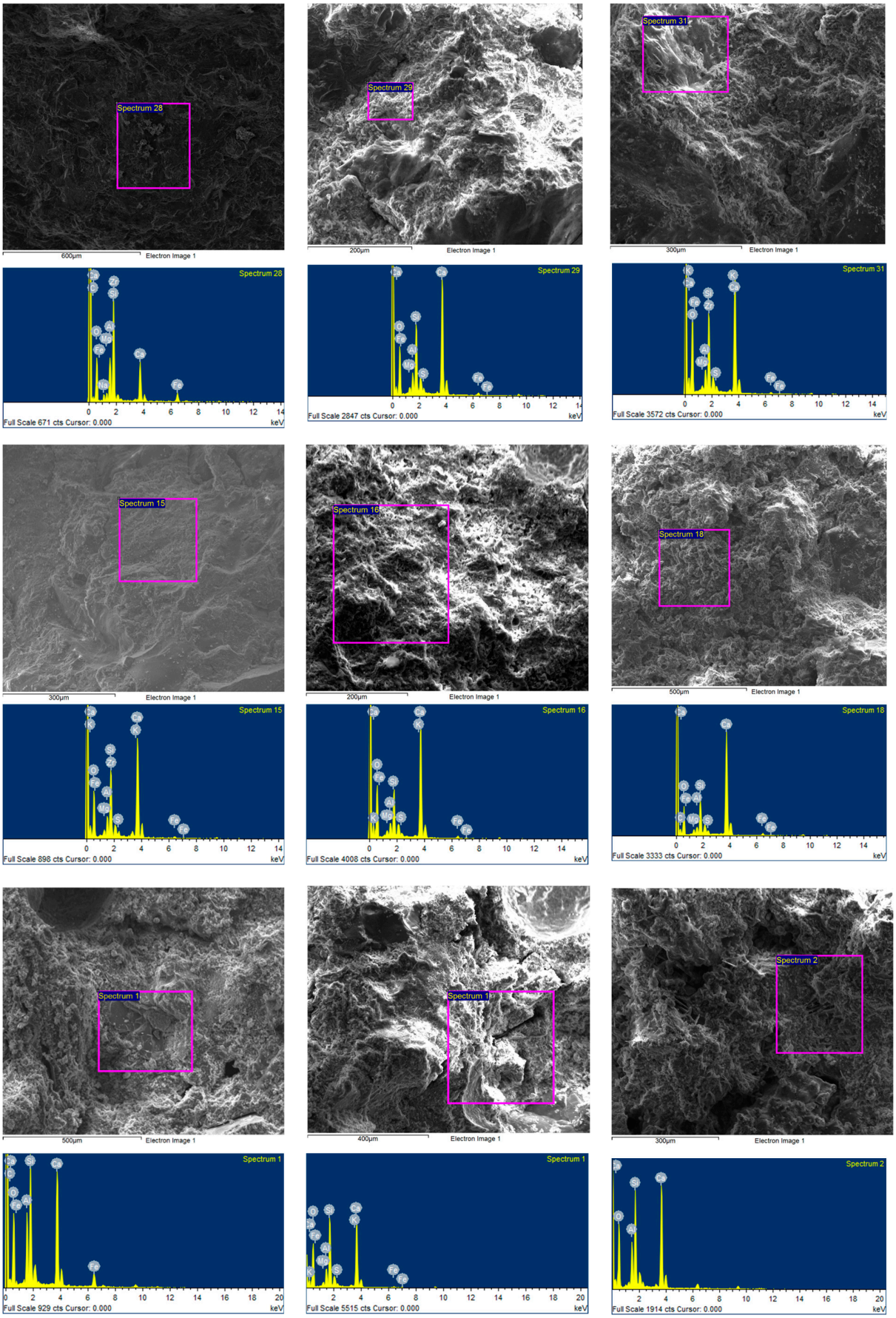


**Figure 16.** *Cont.*

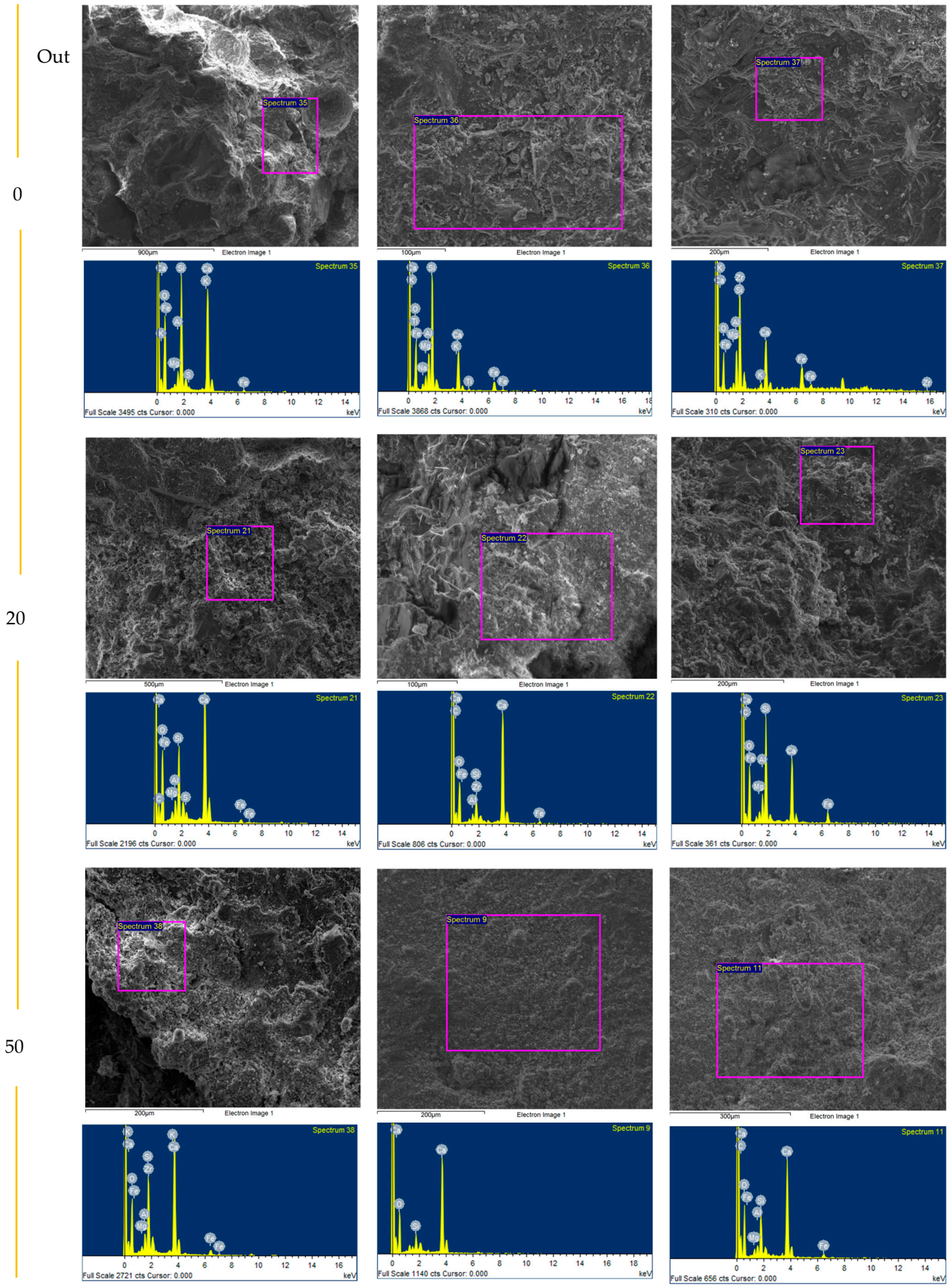


**Figure 16.** EDS (energy-dispersive X-ray spectroscopy) data for India's concrete samples, in the center (IN) and on the border (OUT) of the concrete samples 0%, 20%, and 50% of CBA, before coating.

The EDS results (Figure 14) confirm that in mixtures containing CBA, an increased frequency of Si-rich spectra was observed. In paste-dominated regions, some analyses indicated moderately reduced Ca/Si ratios, which may be consistent with the presence of siliceous fines and/or secondary C–S–H formation. However, Si/Al-rich spectra may also originate from aluminosilicate aggregates or unreacted ash particles [53,54]. The EDS chemical of 0% CBA concrete analysis is dominated almost exclusively by calcium (Ca) and oxygen (O). Multiple spectra show Ca approx. 44–46 wt% and Si approx. 0–1 wt%. For 20% CBA, the appearance of Al and Si confirms the presence of CBA particles within the matrix. However, the Ca levels remain relatively high in many spots, suggesting that while CBA is present, the pozzolanic reaction is limited. This aligns perfectly with the SEM observation of "marginal densification" as the chemical "ingredients" (Si and Al) are present, but their concentration at 20% replacement is insufficient to chemically convert the bulk of the cement paste, leaving the microstructure largely similar to the 0% CBA concrete. For the 50% CBA, several spectra reveal silicon (Si) levels of 15–20 wt%, a massive increase compared to the 0% CBA. This high Si content co-located with Ca confirms the formation of secondary calcium–silicate–hydrate (C-S-H) gel. The CBA has successfully released silica, which reacted with the calcium (consuming the weak Portlandite) to form this durable binder. This chemical data explains the "smooth, dense, homogeneous" surface seen in the SEM. The secondary C-S-H gel detected by EDS physically fills the voids, creating the discontinuous pore network that led to the lowest chloride migration coefficient.

Concomitantly, the difference between the samples IN and OUT, in the SEM/EDS, detects environmental interactions at the concrete surface. Across the samples (particularly 20% and 50% CBA OUT), there are spectra showing significant carbon (C) content (e.g., 14–24 wt% C). This indicates carbonation at the border of the samples; while carbonation can densify the surface skin (potentially lowering water absorption slightly), the core durability (measured by "IN" chemistry) is driven by the CBA content.

Figure 15 presents the SEM analysis of the center (IN) and on the border (OUT) of the concrete samples 0%, 20%, and 50% of CBA, produced in India, before coating.

Overall, according to Figure 15, the India 0% CBA shows a highly porous microstructure, with large, connected voids and a wide interfacial transition zone (ITZ). The open network allows rapid chloride ingress. The 20% CBA Indian concrete presents the optimum density, with voids filled and a cohesive matrix. The SEM of 50% CBA shows a disrupted microstructure, with agglomerations and a lack of cohesion.

The microstructure of the India 0% CBA mix appears to be the most open and porous of all the samples discussed so far. This aligns perfectly with it having the highest chloride migration coefficient (16.54). The observed interconnected pore network and porous ITZ provide little resistance to the electric field, allowing chloride ions to migrate rapidly. This confirms why this mix is the worst performer in the study. Therefore, just like the UK sample, this highly porous surface is the ideal candidate for a coating. Unlike the UK concrete (where 20% CBA showed little effect), the Indian concrete with 20% CBA displays a clear and significant transformation in its microstructure compared to the 0% control. The most striking difference compared to the 0% CBA images is the reduction in large capillary pores. The matrix appears significantly more cohesive. The large, open voids seen in the control mix have been filled or segmented. The densification observed in the SEM images correlates with the drop in capillary absorption (from approx. 13.5 to approx. 6.0 $kg/m^2$). The interconnected channels required for capillary suction have been effectively blocked. The SEM images for the 50% CBA Indian concrete reveal a microstructure that is visibly different from the dense, cohesive 20% mix. The high volume of CBA fines appears to have disrupted the matrix homogeneity rather than refining it further. Unlike the uniform matrix seen in the 20% mix, the 50% mix appears disjointed. The sheer volume of replacement

material seems to have exceeded the capacity of the cement paste to effectively bind everything together.

Figure 16 shows the EDS results for Indian concrete, in the center (IN) and on the border (OUT) of the concrete samples 0%, 20% and 50% of CBA, before coating.

For the concrete produced in India with 0% CBA, the analysis of the IN and OUT zones through EDS shows that the OUT zone looks slightly more Si/Al-rich and less Ca-dominant than IN (where IN shows Ca approx. 44–54 wt% and O approx. 45–54 wt% with negligible silicon (<1%)), in line with surface alteration. The IN retains classic CH-rich signatures. The 20% CBA composition shows the most refined microstructure overall, with IN being dense and Ca being moderated by pozzolanic reaction; OUT is further decalcified but remains gel-dominant. The 50% CBA shows strong evidence of incomplete reaction and heterogeneity—where ash signatures dominate, with lower Ca availability. This often correlates with higher residual porosity and variable performance, especially near the border.

### 3.4.2. After Coating

The following Figure 17 presents the SEM results for the UK concrete after CNM coating.

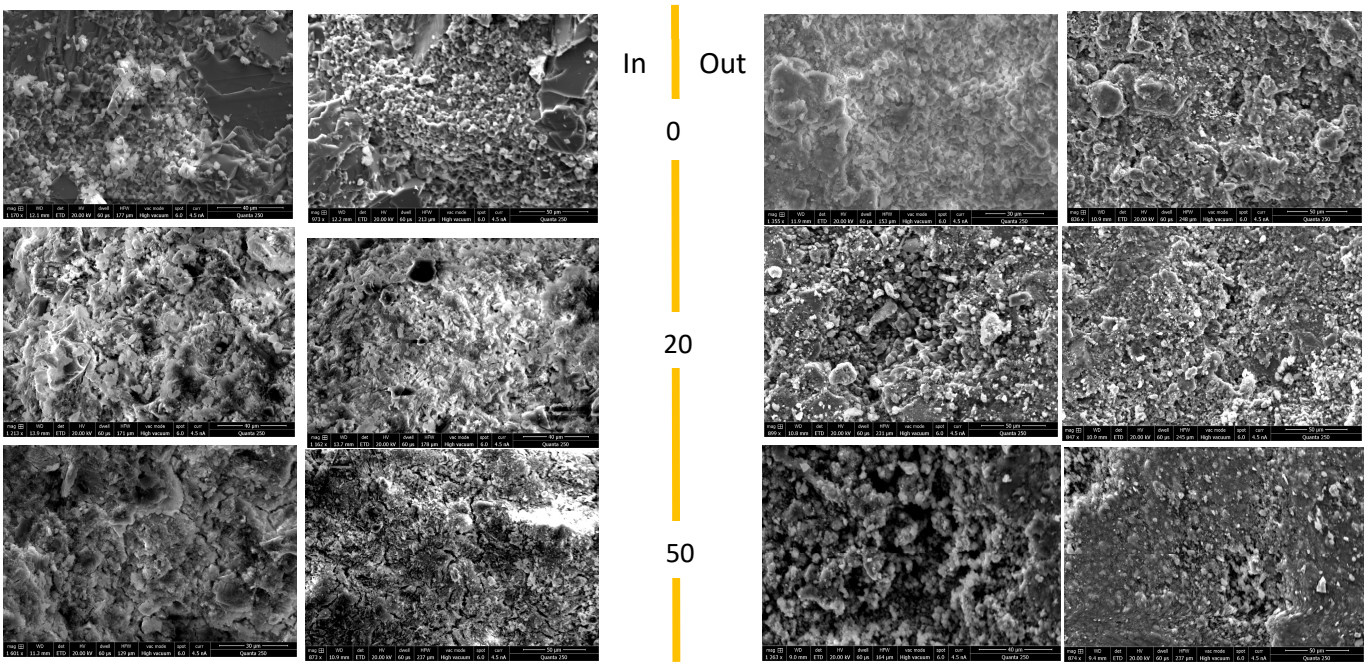


**Figure 17.** Analysis of the center (IN) and on the border (OUT) of the coated concrete samples 0%, 20% and 50% of CBA, produced in the UK, after CNM coating.

The CNM coating (Figures 17 and 18) significantly reduces visible surface porosity in all mixes, especially at borders, with clear improvement in sealing microcracks and ITZ gaps. The 20% CBA + CNM shows the most uniform and dense microstructure, ideal for durability. However, at 50% CBA, CNM helps but cannot fully overcome substrate heterogeneity. The results show that after CNM coating, OUT zones are frequently Ca-dominant (high Ca/Si; elevated Ca/(Si + Al)), consistent with portlandite/calcite surfaces now stabilized/sealed by CNM. The EDS results show that after CNM, the Al/Si rises and Ca indices moderate at 20% IN, matching SEM evidence of dense gel; coating complements pozzolanic refinement.

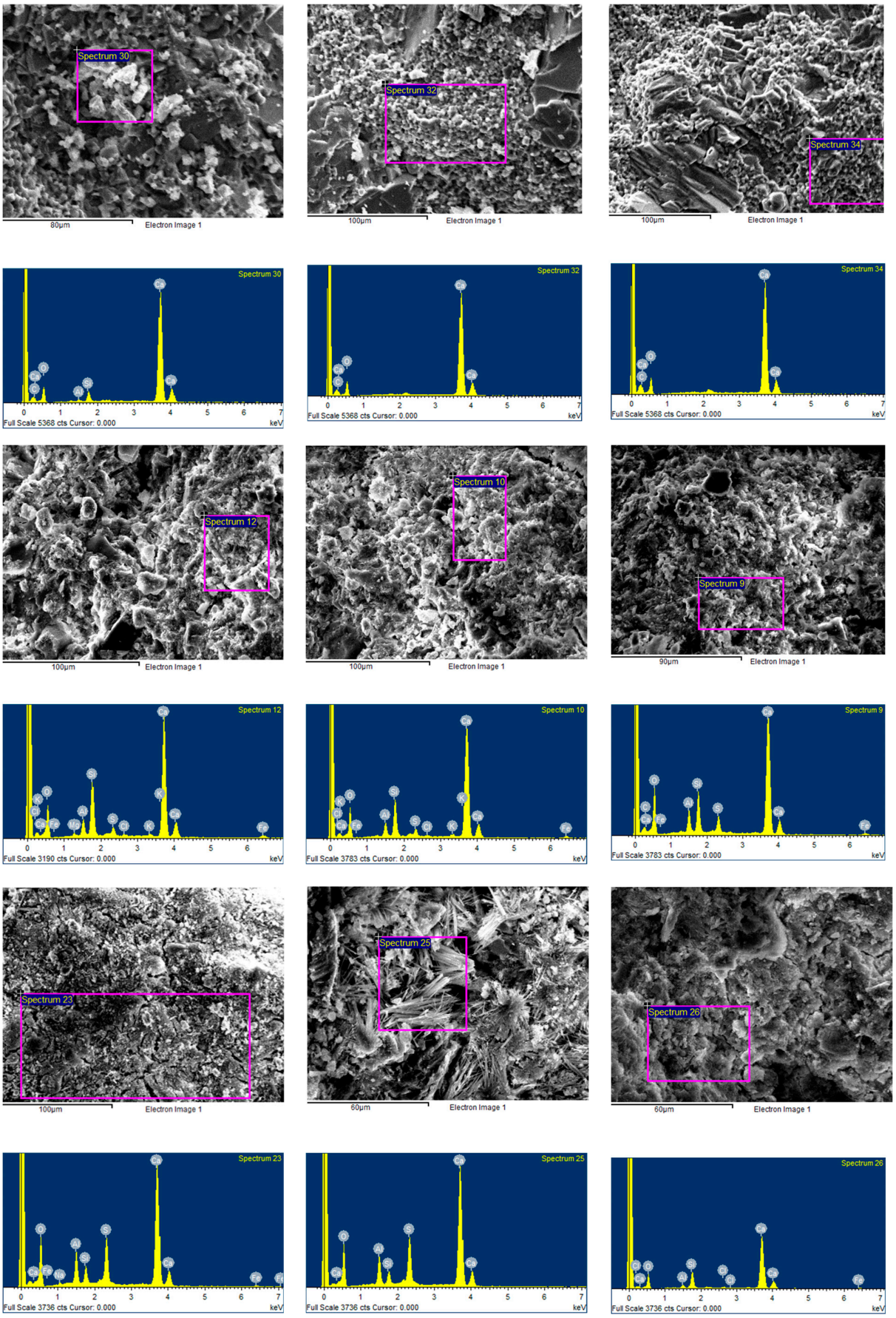


**Figure 18.** *Cont.*

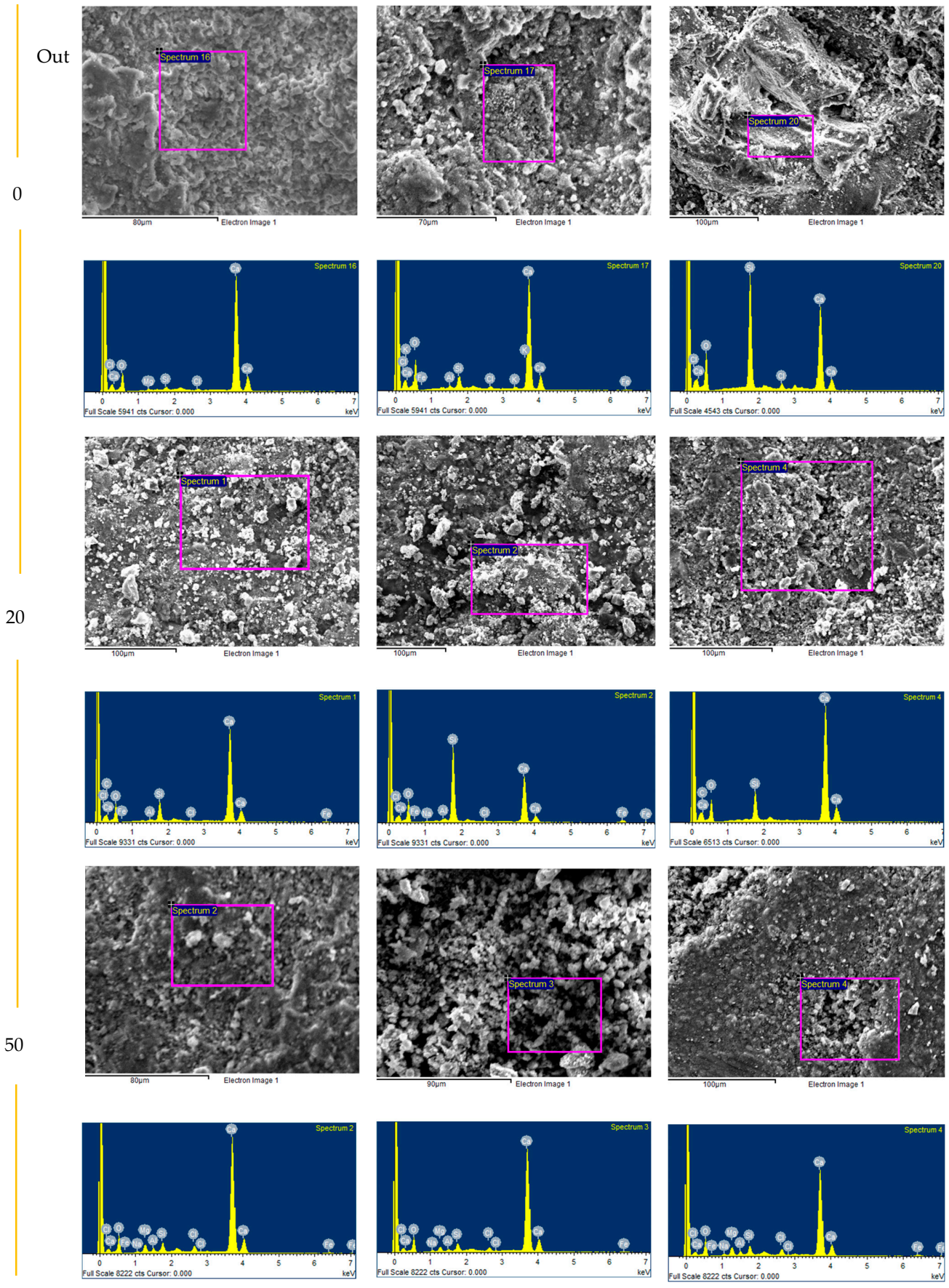


**Figure 18.** EDS (energy-dispersive X-ray spectroscopy) data for the UK's coated concrete, in the center (IN) and on the border (OUT) of the concrete samples 0%, 20% and 50% of CBA, after CNM coating.

The compassion of UK concrete before and after CNM coating shows that for 0%CBA the surface was dominated purely by calcium (Ca) and oxygen (O) (portlandite/calcite). After the coating, the high carbon detected comes almost exclusively from the CNM coating. The EDS (Figure 18) confirms that a thick, substantial coating layer was absorbed by the porous 0% surface, directly explaining the 67.7% reduction in chloride migration. For the 20% CBA, while the before-coated samples had spots of carbonation, the CNM-coated concrete shows a consistently high carbon signal, indicating a uniform organic film covering the surface. The coating is present and continuous, providing a 55.2% improvement in durability.

However, the results show that in 50% CBA concrete, the coating does not form a very thin film on a less dense mix than this one. According to SEM/EDS, the before-coating sample surface was already heavily carbonated or chemically complex in certain areas. After the CNM coating, there is no massive spike in carbon compared to the carbonated baseline before coating. In fact, the carbon signal is lower than the peak values found before coating. Therefore, this lack of a massive, new carbon signature suggests the coating did not form a thick, absorbed layer (unlike the 0% mix). It likely formed a thin surface film on the already dense substrate, explaining why it offered the lowest additional durability benefit (15.7%).

The following figures (Figures 19 and 20) show the SEM/EDS for the bacteria-based self-healing coating on the Indian concrete.

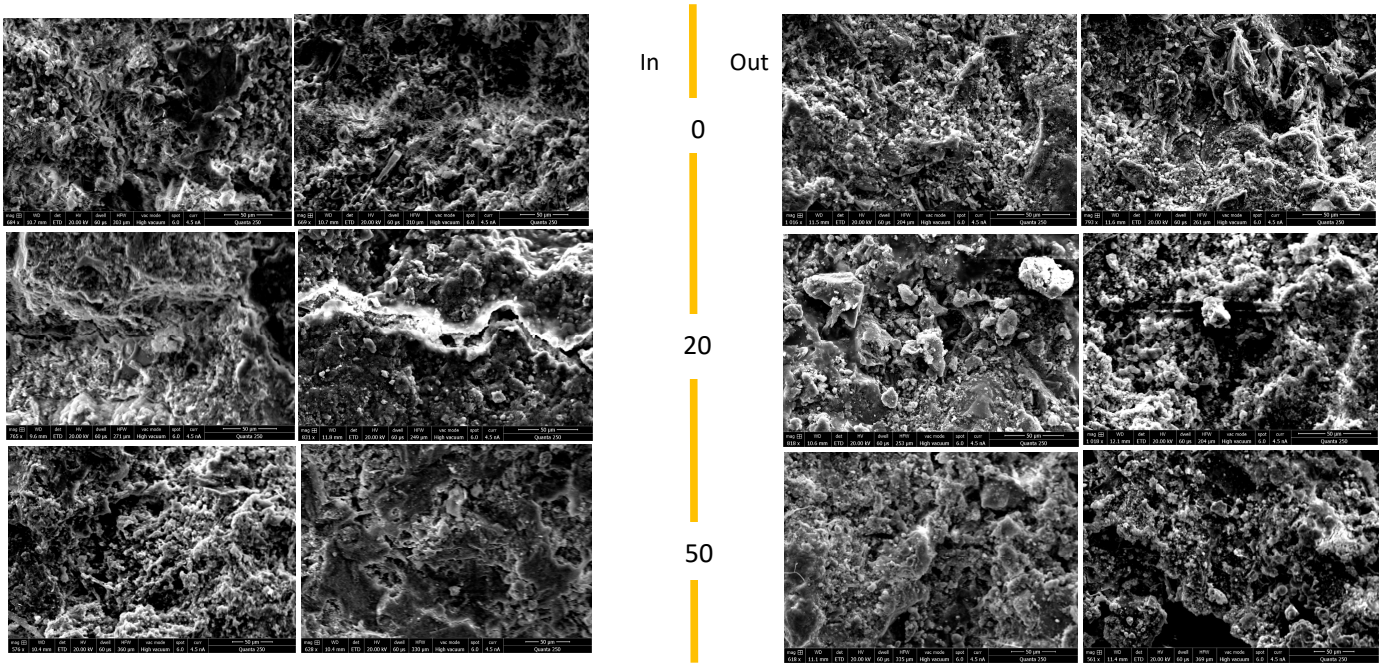


**Figure 19.** Analysis of the center (IN) and on the border (OUT) of the coated concrete samples 0%, 20%, and 50% of CBA, produced in India, after the bacteria-based self-healing coating.

EDS results (Figure 19) for 0% CBA show that self-healing coating introduces Aluminate Ferrite Trisulfate (Aft)/Aluminate Ferrite Monosulfate (AFm) signatures in the interior and reduces Ca dominance at the border, consistent with biogenic sealing of pores and ion redistribution. For 20% of CBA, most balanced interior gel (pozzolanic) with self-healing coating, adding selective AFt/AFm at the surface, consistent with SEM observations (Figure 18) of dense gel with pore infills in coated systems. However, for 50% CBA, the self-healing coating heals the surface via sulphate-bearing phases, but the interior remains heterogeneously Si–Al rich; overall chemistry still reflects Ca limitation relative to 20%.

In

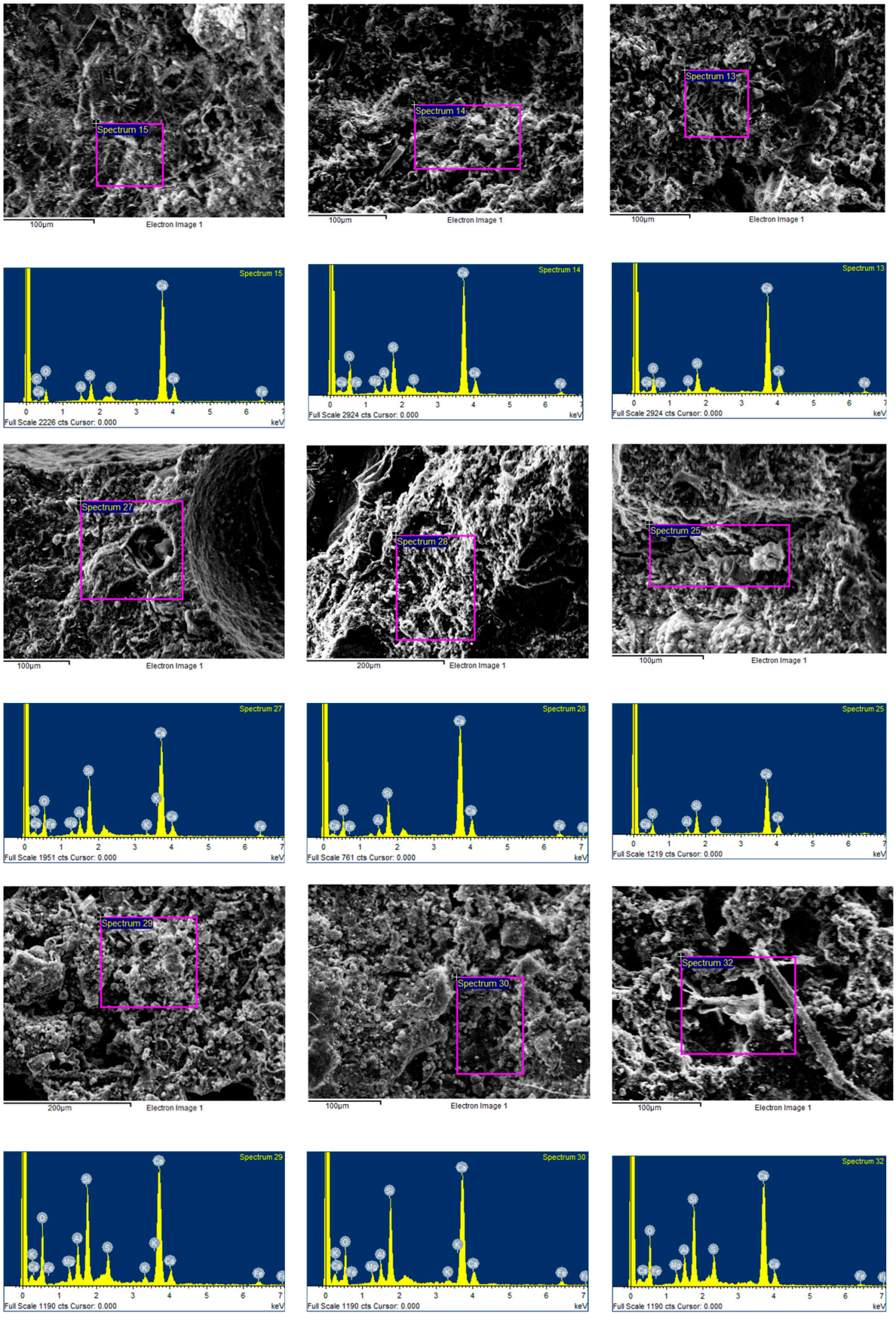


**Figure 20.** *Cont.*

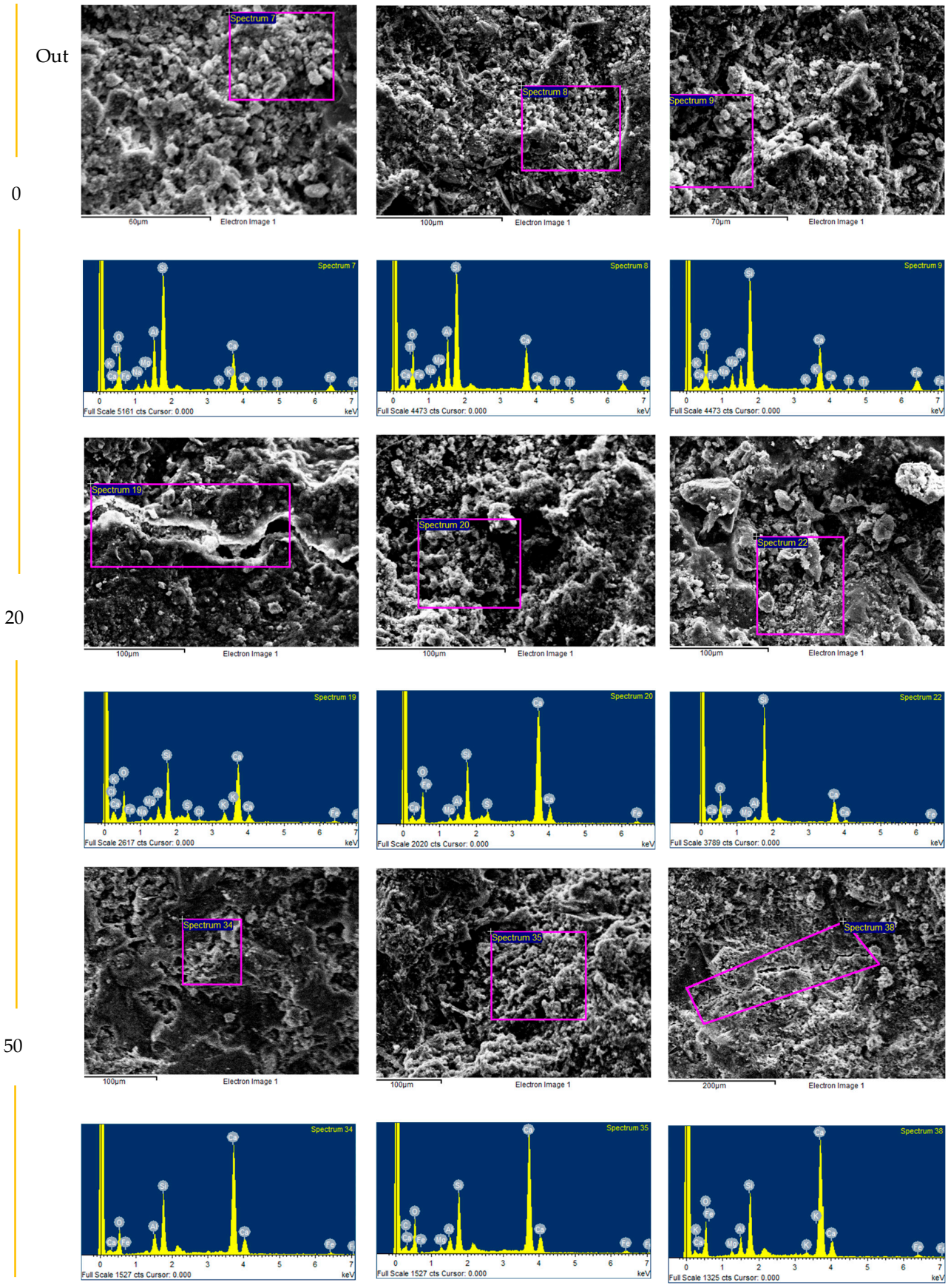


**Figure 20.** EDS (energy-dispersive X-ray spectroscopy) data for India's coated concrete, in the center (IN) and on the border (OUT) of the concrete samples 0%, 20% and 50% of CBA, after bacteria-based self-healing coating.

The EDS presented in Figure 20 shows that for all mixes, OUT zones show lower Ca/Si than IN, consistent with surface leaching/carbonation plus self-healing coating precipitation (which can trap ions near the surface). Relative to "before coating" (Figures 15 and 16), the self-healing coating shifts OUT chemistry toward higher S/Al at borders and moderates Ca signals, while IN chemistry at 20% remains pozzolanic-refined. This matches the expectation that bacteria-based systems precipitate mineral phases in exposed pores and seal microcracks preferentially near the surface. *Shewanella* spp. are facultative anaerobes that respire Fe(III) when oxygen is scarce, using outer-membrane decaheme cytochromes (MtrC/OmcA) and the Mtr electron-transfer pathway to reduce extracellular Fe(III) oxides to Fe(II). This consumes oxidants and promotes carbonate biomineralisation that seals cracks and diminishes porosity, which reduces corrosion risk. Under carbonate-rich conditions (as in self-healing), Fe(II) can precipitate as siderite ($FeCO_3$); with phosphate available, vivianite ($Fe_3(PO_4)_2 \cdot 8H_2O$) can form—both are dense, protective ferrous minerals. Recent concrete-focused work shows iron-reducing bacteria (including *Shewanella*) can biogenically produce siderite/vivianite layers on iron substrates that act as corrosion-mitigating barriers. This compositional change shows the deposition of calcium-rich compounds within pores, most likely $CaCO_3$, due to microbial activity. Mineral precipitation is a bacterial self-healing technique that has been shown to partially fill cracks and pores according to the literature [20,55]. The higher Ca/Si ratio in coated samples provides support to the idea that new healing products are developing the inside microstructure. Elevated Ca/Si values, compared to uncoated samples, indicate localized enrichment of calcium relative to silicon, which is consistent with the precipitation of Ca-rich phases such as calcite and portlandite, as well as sulphate–aluminate hydrates (AFt/AFm) detected at the surface These findings are consistent with SEM evidence of partial pore filling, indicating that the self-healing coating improves microstructural compactness, while its healing capacity is limited to smaller voids.

### *3.5. Chemical and Mineralogical Characterization (XRF and XRD)*

#### 3.5.1. XRF

The following Table 4 shows the XRF major-oxide composition (wt%) table for all compositions. The coal-biomass ash (CBA) utilized as a substitute for fine aggregate is chemically comparable to coal fly ash, with high silica and alumina content, as well as significant alkali and phosphate levels [56]. Usually, coal-fired biomass ashes include more calcium, magnesium, potassium, and phosphorus than pure coal ash [12,56]. XRF shows the expected shift toward a silico-aluminous chemistry as CBA increases ($SiO_2$ and $Al_2O_3$ rising, CaO proportionally moderated), while stratified sampling reveals coating-induced surface signatures. After CNM, UK outer powders exhibit Ca-rich and Cl-bearing composition, consistent with SEM/EDS evidence of Ca-rich crusts and halide retention under the coating. After the bacteria-based coating, India's outer powders—particularly at 50% CBA—show $SO_3$ enrichment, concordant with AFt/AFm precipitation detected by EDS (high S/Al), while inner powders maintain pozzolanic Si–Al-rich gel chemistry (moderate Ca/Si and elevated Al/Si). Together, the XRF bulk trends and the EDS local signatures confirm that coatings drive Ca-rich and sulphate–aluminate healing products at surfaces, whereas ash-enhanced gels dominate interiors, explaining the observed microstructural densification and improved durability.

**Table 4.** Major oxide composition (wt%) of the tested concrete samples before/after bio-coating.

| Chemical Composition | | $CO_2$ | $SiO_2$ | CaO | $Al_2O_3$ | $Fe_2O_3$ | $K_2O$ | $P_2O_5$ | MgO | $SO_3$ | $TiO_2$ | Cl |
|---|---|---|---|---|---|---|---|---|---|---|---|---|
| India | 0% | 37.5 | 27.2 | 23.5 | 4.68 | 3.48 | 0.793 | 0.0721 | 1.26 | 0.894 | 0.399 | 0.026 |
| Before | 20% | 43.1 | 25.8 | 21.2 | 4.49 | 2.27 | 0.652 | 0.0796 | 1.07 | 0.901 | 0.244 | 0.017 |
| (Outer) | 50% | 37.2 | 29.6 | 21.3 | 5.77 | 2.68 | 0.576 | 0.117 | 1.12 | 1.05 | 0.352 | 0.033 |
| UK | 0% | 44 | 10.8 | 40.7 | 1.8 | 0.916 | 0.242 | 0.0265 | 0.446 | 0.791 | 0.094 | 0.024 |
| Before | 20% | 41.6 | 12.6 | 40.2 | 2.28 | 1.12 | 0.236 | 0.0332 | 0.474 | 1.07 | 0.129 | 0.030 |
| (Outer) | 50% | 40.7 | 14.7 | 38.3 | 2.81 | 1.32 | 0.297 | 0.0391 | 0.468 | 0.971 | 0.154 | 0.026 |
| India | 0% | 36.7 | 28.3 | 23.6 | 4.5 | 3.21 | 0.862 | 0.073 | 1.12 | 0.936 | 0.409 | 0.032 |
| Before | 20% | 40.2 | 26.4 | 20.8 | 5.34 | 3.54 | 0.811 | 0.098 | 1.25 | 0.818 | 0.464 | 0.013 |
| (Inner) | 50% | 32.4 | 31.7 | 23.2 | 5.96 | 3 | 0.656 | 0.124 | 1.15 | 1.24 | 0.343 | 0.032 |
| UK | 0% | 50.4 | 8.14 | 38.2 | 1.25 | 0.69 | 0.206 | 0.018 | 0.315 | 0.563 | 0.067 | 0.024 |
| Before | 20% | 42.5 | 11.9 | 40.5 | 2.09 | 1.06 | 0.295 | 0.027 | 0.435 | 0.897 | 0.112 | 0.022 |
| (Inner) | 50% | 38 | 13.8 | 42 | 2.7 | 1.3 | 0.319 | 0.039 | 0.491 | 0.954 | 0.160 | 0.023 |
| India | 0% | 45.4 | 25.8 | 19.1 | 3.97 | 2.69 | 0.726 | 0.060 | 0.971 | 0.724 | 0.294 | 0.012 |
| After | 20% | 40 | 28.5 | 20 | 5.19 | 2.98 | 0.763 | 0.092 | 1.14 | 0.764 | 0.362 | 0.020 |
| (Outer) | 50% | 28.7 | 36 | 20.9 | 6.78 | 3.83 | 0.803 | 0.150 | 1.4 | 0.663 | 0.501 | 0.014 |
| UK | 0% | 40.1 | 8.29 | 47.2 | 1.65 | 0.816 | 0.181 | 0.021 | 0.452 | 0.727 | 0.071 | 0.281 |
| After | 20% | 39.9 | 10.5 | 44.7 | 1.95 | 1.08 | 0.214 | 0.017 | 0.119 | 0.83 | 0.104 | 0.384 |
| (Outer) | 50% | 42.8 | 9.96 | 42.3 | 2.08 | 1.03 | 0.211 | 0.028 | 0.394 | 0.681 | 0.116 | 0.247 |
| India | 0% | 39.7 | 29 | 20.3 | 4.6 | 3.02 | 0.812 | 0.067 | 1.13 | 0.807 | 0.368 | 0.011 |
| After | 20% | 39 | 29.6 | 19.4 | 5.36 | 3.11 | 0.836 | 0.083 | 1.16 | 0.794 | 0.361 | 0.016 |
| (Inner) | 50% | 28.4 | 34.9 | 23.6 | 6.75 | 2.73 | 0.781 | 0.126 | 1.21 | 0.926 | 0.375 | 0.019 |
| UK | 0% | 42.4 | 6.65 | 47.5 | 1.45 | 0.641 | 0.163 | 0.018 | 0.399 | 0.579 | 0.056 | 0.079 |
| After | 20% | 39.9 | 13.2 | 40.9 | 2.58 | 1.15 | 0.256 | 0.030 | 0.46 | 0.999 | 0.112 | 0.281 |
| (Inner) | 50% | 38.9 | 10.4 | 45.2 | 2.33 | 1.06 | 0.218 | 0.029 | 0.453 | 0.756 | 0.119 | 0.333 |

#### 3.5.2. XRD

The diffractograms shown in Figures 21 and 22 show the XRD results for 20% CBA Indian concrete (before and after the bacteria-based self-healing coating) and UK concrete (before and after the CNM coating). The dominant binder-related crystalline phases identified were portlandite ($Ca(OH)_2$) and calcite ($CaCO_3$), consistent with hydration and partial carbonation. Quartz and feldspar-family reflections are primarily attributed to natural aggregates and/or crystalline remnants present in the coal–biomass ash. Minor reflections were tentatively assigned to additional silicate or spinel-type phases that may originate from high-temperature combustion products within the ash [53,57,58].

The XRD data in Figure 21 shows a clear decrease in portlandite (CH) and no bulk increase in AFt/AFm peaks, which suggests that the bacteria-based coating actively modified the mineralogy, consuming CH and likely forming calcite and localized AFt/AFm in cracks and pores. AFt/AFm phases were considered in the mechanistic discussion because they are established chloride-binding hydrates in OPC systems. However, in the present bulk XRD patterns, no unambiguous AFt/AFm reflections could be confidently identified, likely due to their low abundance and overlapping with other phases in powdered concrete specimens [59–61]. This aligns with the idea of bio-induced healing and $CaCO_3$ precipitation as a crack-sealing mechanism. In the concrete before coating, different concentrations of calcite, quartz, and portlandite were observed. Calcite appeared to be the main carbonate phase, indicating that portlandite had been partially carbonated. Quartz, produced from aggregates and CBA, was the most stable silicate phase, with portlandite confirming continuous hydration processes. Significant alterations in the self-healing coating included a decrease in calcite intensity, the partial elimination of weaker peaks, and the full loss of portlandite reflections. Quartz reflections became more prominent and

numerous new minor crystalline phases emerged, including orthoclase, calcian enstatite, galaxite, and collinsite. The loss of portlandite indicates active consumption of $Ca(OH)_2$, possibly by pozzolanic interaction with CBA-derived amorphous silica or transformation into other reaction products. The development of small crystalline phases is most likely due to localized reorganization of CBA elements at the coated interface. The reduction in portlandite and changed carbonate peaks suggest that the coating stabilizes $Ca^{2+}$ into secondary reaction products, potentially densifying the surface matrix and lowering permeability. These changes are compatible with self-healing processes in which microstructural modification helps heal cracks and improve durability.

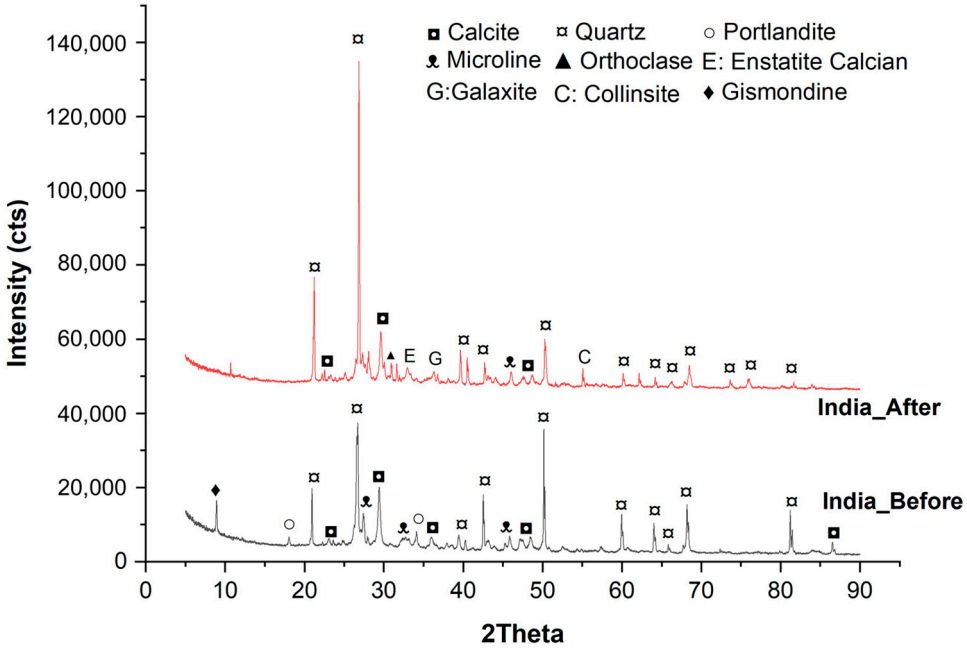


**Figure 21.** XRD Diffractograms of India samples (before/after self-healing coating).

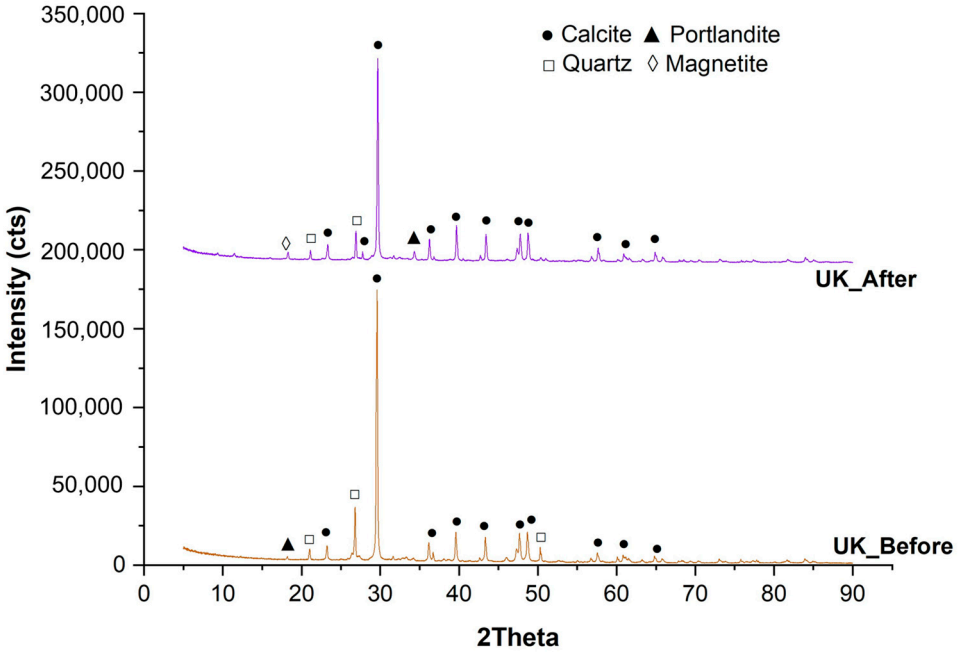


**Figure 22.** XRD Diffractograms of UK samples (before/after cinnamaldehyde coating).

The XRD data in Figure 22 after CNM coating shows a slight increase at ~11.2° (AFm window) and decreases in AFt and CH. In OPC systems, chloride binding can occur through incorporation of $Cl^-$ into AFm-family layered phases, leading to the formation of chloride-bearing Afm, such as Friedel's salt. Thus, Friedel's salt is a product of chloride interaction with AFm, rather than a precursor phase. The primary phases of cinnamaldehyde-coated concrete remained calcite, quartz, and portlandite. While calcite intensity reduced slightly when compared to the control, quartz reflections remained with minor reductions in peak counts. The persistence of portlandite only shows minor new crystalline phases. This means that cinnamaldehyde is not reacting directly to make new mineral products, which are identifiable by XRD. But it protects itself by creating an organic barrier and inhibiting corrosion, not by changing the mineralogy, which stops aggressive ions from getting through. This interpretation is consistent with the performance data, which show that cinnamaldehyde coatings improved resistance to chloride ingress while preserving the alkalinity of the cementitious matrix.

The XRD results show that the bacteria-based self-healing coating promotes phase transformation, proven specifically for portlandite consumption and the formation of secondary crystalline products. Therefore, the bacteria-based coating supports its healing functionality through matrix densification and potential crack sealing through carbonate deposition. However, the cinnamaldehyde coating largely serves as a protective barrier, with minimal crystalline modification, conserving current hydration products while decreasing external degradation threats. The differences in phase evolution emphasize the complementary functions of bio-induced self-healing and organic inhibitory coatings in improving the durability of concretes that are modified by coal-fired biomass ash.

It should be noted that the present experimental design intentionally planned different bio-inspired coatings with distinct concrete systems to reflect context-specific durability priorities rather than to provide a direct comparison between coating types. While this approach enables evaluation of coating–substrate interactions under realistic conditions, direct comparison of self-healing and cinnamaldehyde coatings on identical substrates was beyond the scope of this study. Future work will therefore focus on symmetrical testing, applying both coatings to both concrete systems, to enable direct performance comparison and further validate the observed mechanisms.

## 4. Conclusions

This study demonstrates that incorporating coal-fired biomass ash (CBA) as a fine aggregate replacement can significantly enhance sustainability in concrete production. For Indian concrete, the optimum performance was achieved at 20% CBA, where compressive strength was maintained, and durability improved. At 50% CBA, India mixes exhibited increased porosity and reduced strength, making them highly dependent on surface treatments for durability. However, the UK concrete tolerated higher CBA levels: at 50% replacement, chloride resistance improved markedly due to enhanced pore refinement, although strength reduction still occurred.

Among the two bio-inspired coatings evaluated, the bacteria-based self-healing coating was most effective for India mixes, reducing water absorption by over 80% and sealing microcracks through calcium carbonate precipitation. This mechanism provided long-term moisture protection, which is critical for mixes with higher porosity. However, the cinnamaldehyde coating delivered superior chloride migration resistance for UK mixes, reducing migration coefficients by up to 68%. Its hydrophobic effect, however, was temporary, indicating that CNM is best suited for environments where chloride ingress is the dominant threat rather than prolonged water exposure.

The self-healing coating is a superior waterproofing agent (excellent against capillary suction). Its poor and inconsistent performance in the $D_{nssm}$ 50% CBA suggests that the bacteria-based system or its associated binding agent fails to provide a consistent electrical barrier under the accelerated voltage conditions, especially when dealing with the complex pore structure of the 50% CBA mix.

The CNM coating is a superior ionic barrier (excellent against electrical migration). Its failure in the capillary test means it is not effective as a water repellent surface coating. Its mechanism appears to be primarily related to forming a layer that either impedes the electrical migration path of the chloride ions or offers specific pore blocking only at the micro-level sufficient to stop ionic movement, without eliminating the macroscopic capillary suction of bulk water. The CNM coating acts as a barrier layer, reducing permeability and ingress. Combined with optimal CBA content (20%), it offers maximum protection against carbonation, chloride attack, and moisture penetration. However, at high CBA (50%), CNM improves surface properties, but bulk weaknesses remain.

This study was limited to small-scale laboratory specimens and short-term durability tests. Hence, the real-world performance of these coatings under weathering, cyclic loading, and environmental exposure remains uncertain. Future research should focus on long-term field evaluations, hybrid self-healing and corrosion-mitigating systems, extended durability metrics, and optimization of coating formulations and bacterial efficiency for sustainable large-scale applications.

**Author Contributions:** Conceptualization, N.D.R. and A.B.; methodology, N.D.R., A.B. and M.A.V.; validation, A.B.; formal analysis, N.D.R., M.G., A.B. and F.G.; investigation, N.D.R., Z.Y. and A.B.; resources, R.V.R.; data curation, Z.Y.; writing—original draft preparation, N.D.R.; writing—review and editing, M.A.V., Z.Y., R.V.R., M.G., F.G. and A.B.; visualization, M.G. and F.G.; supervision, A.B.; project administration, A.B.; funding acquisition, A.B. All authors have read and agreed to the published version of the manuscript.

**Funding:** This work is supported by the Marie Sklodowska-Curie Action (MSCA) Postdoctoral Fellowship and UK Research and Innovation (UKRI) under Engineering and Physical Sciences Research Council (EPSRC) [grant number EP/Y015959/1] and by the QR Policy Support Impact Funding "Smart shelters & sustainable futures—Maharashtra's bio-concrete Initiative" CC223010/SoF HESA/H0010 000ABC.

**Institutional Review Board Statement:** Not applicable.

**Informed Consent Statement:** Not applicable.

**Data Availability Statement:** The original contributions presented in the study are included in the article, further inquiries can be directed to the corresponding authors.

**Acknowledgments:** We would like to acknowledge with much appreciation the crucial role of the technical staff of BEST Research Institute.

**Conflicts of Interest:** The authors declare no conflict of interest.

## References

1. Koch, G.; Varney, J.; Thompson, N.; Moghissi, O.; Gould, M.; Payer, J. *International Measures of Prevention, Application, and Economics of Corrosion Technologies Study*; NACE International: Houston, TX, USA, 2016.
2. Mohammed, H.; Ortoneda-Pedrola, M.; Nakouti, I.; Bras, A. Experimental characterisation of non-encapsulated bio-based concrete with self-healing capacity. *Constr. Build. Mater.* **2020**, *256*, 119411. [CrossRef]
3. Bras, A.; van der Bergh, J.; Mohammed, H.; Nakouti, I. Design Service Life of RC Structures with Self-Healing Behaviour to Increase Infrastructure Carbon Savings. *Materials* **2021**, *14*, 3154. [CrossRef]
4. Gagg, C.R. Cement and concrete as an engineering material: An historic appraisal and case study analysis. *Eng. Fail. Anal.* **2014**, *40*, 114–140. [CrossRef]

5. Andrew, R.M. Global $CO_2$ emissions from cement production, 1928–2018. *Earth Syst. Sci. Data* **2019**, *11*, 1675–1710. [CrossRef]
6. Maj, I.; Niesporek, K.; Płaza, P.; Maier, J.; Łój, P. Biomass Ash: A Review of Chemical Compositions and Management Trends. *Sustainability* **2025**, *17*, 4925. [CrossRef]
7. van der Bergh, J.M.; Miljević, B.; Vučetić, S.; Šovljanski, O.; Markov, S.; Riley, M.; Ranogajec, J.; Bras, A. Comparison of Microbially Induced Healing Solutions for Crack Repairs of Cement-Based Infrastructure. *Sustainability* **2021**, *13*, 4287. [CrossRef]
8. Camia, A.; Giuntoli, J.; Jonsson, R.; Robert, N.; Cazzaniga, N.E.; Jasinevičius, G.; Avitabile, V.; Grassi, G.; Barredo, J.I.; Mubareka, S. *The Use of Woody Biomass for Energy Purposes in the EU, EUR 30548 EN*; Publications Office of the European Union: Luxembourg, 2021; JRC122719. [CrossRef]
9. Ram, S.; Pradhan, K.; Ralegaonkar, R. Use of co-fired blended ash in the development of sustainable construction materials. *Proc. Inst. Civ. Eng.-Eng. Sustain.* **2018**, *171*, 425–432. [CrossRef]
10. Lanjewar, B.A.; Chippagiri, R.; Dakwale, V.A.; Ralegaonkar, R.V. Development of bio-based blended ash and fly ash-based alkali-activated concrete. *Mag. Concr. Res.* **2023**, *75*, 1202–1211. [CrossRef]
11. Wang, S.; Miller, A.; Llamazos, E.; Fonseca, F.; Baxter, L. Biomass fly ash in concrete: Mixture proportioning and mechanical properties. *Fuel* **2008**, *87*, 365–371. [CrossRef]
12. Teixeira, E.R.; Camões, A.; Branco, F.G. Synergetic effect of biomass fly ash on improvement of high-volume coal fly ash concrete properties. *Constr. Build. Mater.* **2022**, *314*, 125680. [CrossRef]
13. Zhao, H.; Wang, Q.; Shang, R.; Li, S. Development, Challenges, and Applications of Concrete Coating Technology: Exploring Paths to Enhance Durability and Standardization. *Coatings* **2025**, *15*, 409. [CrossRef]
14. Broomfield, J.P. *Corrosion of Steel in Concrete*; CRC Press: London, UK, 2022. [CrossRef]
15. Andrade, C.; Alonso, C. Test methods for on-site corrosion rate measurement of steel reinforcement in concrete by means of the polarization resistance method. *Mater. Struct.* **2004**, *37*, 623–643. [CrossRef]
16. Bastidas-Arteaga, E.; Stewart, M.G. Damage risks and economic assessment of climate adaptation strategies for design of new concrete structures subject to chloride-induced corrosion. *Struct. Saf.* **2015**, *52*, 40–53. [CrossRef]
17. Jiang, L.; Wu, M.; Du, F.; Chen, D.; Xiao, L.; Chen, W.; Du, W.; Ding, Q. State-of-the-Art Review of Microcapsule Self-Repairing Concrete: Principles, Applications, Test Methods, Prospects. *Polymers* **2024**, *16*, 3165. [CrossRef]
18. Amran, M.; Onaizi, A.M.; Fediuk, R.; Vatin, N.I.; Muhammad Rashid, R.S.; Abdelgader, H.; Ozbakkaloglu, T. Self-Healing Concrete as a Prospective Construction Material: A Review. *Materials* **2022**, *15*, 3214. [CrossRef] [PubMed]
19. Jonkers, H.; Schlangen, E. Development of a bacteria-based self healing concrete. In *Tailor Made Concrete Structures*; Taylor & Francis Group: London, UK, 2008. [CrossRef]
20. Wiktor, V.; Jonkers, H.M. Quantification of crack-healing in novel bacteria-based self-healing concrete. *Cem. Concr. Compos.* **2011**, *33*, 763–770. [CrossRef]
21. Seifan, M.; Samani, A.K.; Berenjian, A. Bioconcrete: Next generation of self-healing concrete. *Appl. Microbiol. Biotechnol.* **2016**, *100*, 2591–2602. [CrossRef] [PubMed]
22. Anjomshoa, E.; Ramezanianpour, A. Sustainable self-healing concrete technologies: A review of bacteria-induced mechanisms and their effects on structural integrity, mechanical properties and durability. *Int. J. Build. Pathol. Adapt.* **2025**, 1–24. [CrossRef]
23. Montemor, M.F. Functional and smart coatings for corrosion protection: A review of recent advances. *Surf. Coat. Technol.* **2014**, *258*, 17–37. [CrossRef]
24. Verma, C.; Ebenso, E.E.; Bahadur, I.; Quraishi, M.A. An overview on plant extracts as environmental sustainable and green corrosion inhibitors for metals and alloys in aggressive corrosive media. *J. Mol. Liq.* **2018**, *266*, 577–590. [CrossRef]
25. Zomorodian, A.; Behnood, A. Review of Corrosion Inhibitors in Reinforced Concrete: Conventional and Green Materials. *Buildings* **2023**, *13*, 1170. [CrossRef]
26. Growcock, F.B. Inhibition of Steel Corrosion in HCl by Derivatives of Cinnamaldehyde. *Corrosion* **1989**, *45*, 1003–1007. [CrossRef]
27. Jafferji, H.; Sakulich, A.R.; Schiffman, J.D. Preliminary study on mitigating steel reinforcement corrosion with bioactive agent. *Cem. Concr. Compos.* **2016**, *69*, 9–17. [CrossRef]
28. Jafferji, H.; Sharifi, N.P.; Schneider, E.M.; Sakulich, A.R. Investigation of incorporating cinnamaldehyde into Lightweight Aggregate for potential corrosion reduction in cementitious materials. *Cem. Concr. Compos.* **2018**, *87*, 1–9. [CrossRef]
29. Ettish, M.N.; El-Sayyad, G.S.; Elsayed, M.A.; Abuzalat, O. Preparation and characterization of new adsorbent from Cinnamon waste by physical activation for removal of Chlorpyrifos. *Environ. Chall.* **2021**, *5*, 100208. [CrossRef]
30. Olivia, M.; Jingga, H.; Toni, N.; Wibisono, G. Biopolymers to improve physical properties and leaching characteristics of mortar and concrete: A review. *IOP Conf. Ser. Mater. Sci. Eng.* **2018**, *345*, 012028. [CrossRef]
31. Chavan, T.K.; Sethi, S.K. Eco-friendly self-cleaning coatings: Fundamentals, fabrication, applications, and sustainability. *J. Mater. Chem. B* **2025**, *13*, 429–453. [CrossRef]

32. Boutouam, Y.; Hayek, M.; Bouarab, K.; Yahia, A. A Comprehensive Review of Plant-Based Biopolymers as Viscosity-Modifying Admixtures in Cement-Based Materials. *Appl. Sci.* **2024**, *14*, 4307. [CrossRef]
33. Shanmugavel, D.; Selvaraj, T.; Ramadoss, R.; Raneri, S. Interaction of a viscous biopolymer from cactus extract with cement paste to produce sustainable concrete. *Constr. Build. Mater.* **2020**, *257*, 119585. [CrossRef]
34. Yehia, S.; Ibrahim, A.M.; Ahmed, D.F. The impact of using natural waste biopolymer cement on the properties of traditional/fibrous concrete. *Innov. Infrastruct. Solut.* **2023**, *8*, 287. [CrossRef]
35. *BS EN 197-1*; Cement. Part 1, Composition, Specifications and Conformity Criteria for Common Cements. British Standards Institution: London, UK, 2011.
36. *BS EN 12620:2013*; Aggregates for Concrete. British Standards Institution: London, UK, 2013.
37. *ASTM C33/C33M-23*; Standard Specification for Concrete Aggregates. ASTM International: West Conshohocken, PA, USA, 2023.
38. *BS 8500-1:2023*; Concrete. Complementary British Standard to BS EN 206—Specification for Constituent Materials and Concrete. British Standards Institution: London, UK, 2023.
39. Tang, P.L.; Cham, X.Y.; Hou, X.; Deng, J. Potential use of waste cinnamon leaves in stirred yogurt fortification. *Food Biosci.* **2022**, *48*, 101838. [CrossRef]
40. Sigma Aldrich. NMR Chemical Shifts of Impurities. Available online: https://www.sigmaaldrich.com/GB/en/product/aldrich/w228613?srsltid=AfmBOoonAnr573TJ1S7Rilc2BTGvXaWAG9-ghq7TVRHx0vh8nxI5HjP (accessed on 2 April 2025).
41. Nordtest, "Concrete, Mortar and Cement-Based Repair Materials: Chloride Migration Coefficient from Non-Steady-State Migration Experiments (NT BUILD 492)," 1999. Available online: https://www.nordtest.info/wp/1999/11/21/concrete-mortar-and-cement-based-repair-materials-chloride-migration-coefficient-from-non-steady-state-migration-experiments-nt-build-492/ (accessed on 13 April 2025).
42. *BS EN 12390-3:2019*; Testing Hardened Concrete—Compressive Strength of Test Specimens. British Standards Institution: London, UK, 2019.
43. *BS EN 1015-18:2002*; Methods of Test for Mortar for Masonry—Determination of Water Absorption Coefficient Due to Capillary Action of Hardened Mortar. British Standards Institution: London, UK, 2002.
44. Aygun, B.F.; Bilir, T.; Uysal, M. Coal bottom ash and its applications in cement and concrete technologies: A review. *Discov. Civ. Eng.* **2024**, *1*, 86. [CrossRef]
45. Park, J.-H.; Bui, Q.-T.; Jung, S.-H.; Yang, I.-H. Selected Strength Properties of Coal Bottom Ash (CBA) Concrete Containing Fly Ash under Different Curing and Drying Conditions. *Materials* **2021**, *14*, 5381. [CrossRef] [PubMed]
46. Siddique, R. Utilization of Industrial By-products in Concrete. *Procedia Eng.* **2014**, *95*, 335–347. [CrossRef]
47. Singh, M.; Siddique, R. Properties of concrete containing high volumes of coal bottom ash as fine aggregate. *J. Clean. Prod.* **2015**, *91*, 269–278. [CrossRef]
48. Suraneni, P.; Burris, L.; Shearer, C.R.; Hooton, R.D. ASTM C618 Fly Ash Specification: Comparison with Other Specifications, Shortcomings, and Solutions. *ACI Mater. J.* **2021**, *118*, 157167. [CrossRef]
49. Mors, R.; Jonkers, H. Effect on Concrete Surface Water Absorption upon Addition of Lactate Derived Agent. *Coatings* **2017**, *7*, 51. [CrossRef]
50. Hossain, S.Z.; Al-Shater, A.; Kareem, S.A.; Salman, A.; Ali, R.A.; Ezuber, H.; Hossain, M.M.; Razzak, S.A. Cinnamaldehyde as a Green Inhibitor in Mitigating AISI 1015 Carbon Steel Corrosion in HCl. *Arab. J. Sci. Eng.* **2019**, *44*, 5489–5499. [CrossRef]
51. Saad, W.; El-Shamy, A.M. Unlocking the Potential of Cinnamaldehyde: A Comprehensive Study on Its Dual Role as an Effective Inhibitor Against Corrosion and Microbial Corrosion of Mild Steel in Saline Environments. *J. Bio Tribo-Corros.* **2024**, *10*, 14. [CrossRef]
52. Silva, R.V.; de Brito, J.; Dhir, R.K. The influence of the use of recycled aggregates on the compressive strength of concrete: A review. *Eur. J. Environ. Civ. Eng.* **2015**, *19*, 825–849. [CrossRef]
53. Kutchko, B.; Kim, A. Fly ash characterization by SEM–EDS. *Fuel* **2006**, *85*, 2537–2544. [CrossRef]
54. Zhang, Y.; Saravanakumar, K.; Çopuroğlu, O. Some Critical Reflections on the SEM-EDS Microanalysis of the Hydrotalcite-like Phase in Slag Cement Paste. *Materials* **2023**, *16*, 3143. [CrossRef] [PubMed]
55. Sierra-Beltran, M.G.; Jonkers, H.M.; Schlangen, E. Characterization of sustainable bio-based mortar for concrete repair. *Constr. Build. Mater.* **2014**, *67*, 344–352. [CrossRef]
56. Sarabèr, A.J. Fly Ash from Coal and Biomass for Use in Concrete: Origin, Properties and Performance. Ph.D. Thesis, Delft University of Technology, Delft, The Netherlands, 2017. [CrossRef]
57. Thomas, M. *Optimizing the Use of Fly Ash in Concrete*; Portland Cement Association: Skokie, IL, USA, 2007.
58. Scrivener, K.; Snellings, R.; Lothenbach, B. (Eds.) *A Practical Guide to Microstructural Analysis of Cementitious Materials*; CRC Press: Boca Raton, FL, USA, 2018. [CrossRef]
59. Lv, J.; Li, D.; Yang, X.; Rong, H.; Xian, C.; Zhang, Z.; Huang, W.; Li, S. Chloride ion binding in cementitious materials: A review of influencing factors and control methods. *Case Stud. Constr. Mater.* **2025**, *22*, e04201. [CrossRef]

60. Georget, F.; Babaahmadi, A.; Machner, A.; Mrak, M.; Dolenec, S.; Xiong, Q.X.; Shiju, J.; Snoeck, D.; Suraneni, P.; Wilson, W. Measuring chloride binding in cementitious materials: A review by RILEM TC 298-EBD. *Mater. Struct.* **2025**, *58*, 348. [CrossRef]
61. Yoon, S.; Ha, J.; Chae, S.R.; Kilcoyne, D.A.; Jun, Y.; Oh, J.E.; Monteiro, P.J. Phase Changes of Monosulfoaluminate in NaCl Aqueous Solution. *Materials* **2016**, *9*, 401. [CrossRef]